A Middle Pleistocene Lower Back and Pelvis from an Aged Human Individual from the Sima de los Huesos Site, Spain

Alejandro BONMATÍ, Asier GÓMEZ-OLIVENCIA, Juan-Luis ARSUAGA, José Miguel CARRETERO, Ana GRACIA, Ignacio MARTÍNEZ, Carlos LORENZO, José María BÉRMUDEZ DE CASTRO, Eudald CARBONELL

Supporting Information (SI) Appendix

Supporting Information I:
Text

Supporting Information II:
Figures

Supporting Information III:
Tables

Supporting Information IV:
References

Supporting Information I: Text

Text S1. Description of the specimens (see also *SI Appendix*, Texts S2, S3, Table S1). ***Pelvis.*** *Right os coxae* (AT-1001 + AT-1002). Almost complete hip bone in three fragments. Two of them are jointly labelled as AT-1001. The largest one represents most of the ilium and ischium. This fragment lacks the bony region around the anterior superior iliac spine (ASIS) and a small cranial portion of the iliac blade. Besides, the sacro-pelvic region has some missing portions (mainly at the posterior border) and is affected by general cracking, but distortion is minimal. The smallest fragment, also labelled as AT-1001, belongs to the lateral portion of the ischio-pubic ramus. This does not fit with the remaining portions of the ischium. The third fragment, labelled as AT-1002, represents most of the pubic body and the inferior pubic ramus. The superior pubic ramus is missing. *Left os coxae* (AT-1000). It is composed of two fragments: a large one preserving most of the ilium and ischium, and another representing most of the pubic bone. The main missing regions are a small cranial portion of the iliac tuberosity, the most anterior superior part of the iliac blade (including the ASIS), and most of the acetabular portion of the pubis. The ventral margin of the anterior inferior iliac spine (AIIS) shows little erosion. *Sacrum and coccyx* (AT-1003). It is composed of a single piece with six vertebral elements. The first sacral vertebra (S1) lacks the ventral parts of the sacral plate and body. Only small portions of the medial crest and ala are absent in the second vertebra (S2), whereas the third vertebra (S3) is slightly damaged on the right lateral part. The fourth and fifth vertebrae lack most of the lateral regions. The sixth element preserves more than the right half body and 1-cm-long lateral transverse process. This last element is considered to represent the partially sacralized first coccygeal vertebra (see *SI Appendix*, Text S2).
Lumbar spine. *First lumbar vertebra (L1)* (VL16=AT-2592+AT-2695+AT-2707+AT-4038+AT-4906). Fragmentary L1 comprising the left half and the dorsal aspect of the vertebral body, both pedicles, the upper left articular facet, both laminae, the lower articular facets and half of the spinous process. *Second lumbar vertebra (L2)* (VL1=AT-2590+AT-2593+AT-2693+AT-2705+AT-2706). Nearly complete albeit fragmentary L2. It is composed of two different fragments that do not fit together: one represents the ventral half of the vertebral body and the second one comprises the dorsal half of the vertebral body and the neural arch. The neural arch lacks the transverse processes and it has suffered erosion of the upper articular facets and left pedicle. *Third lumbar vertebra (L3)* (VL2=AT-2589+AT-2591+AT-2594+AT-2657). Complete L3 except for the left transverse process, and a portion of the dorsal edge of the vertebral body. *Fourth lumbar vertebra (L4)* (VL3=AT-2588+AT-2658). Complete L4 except for the missing transverse processes. *Fifth lumbar vertebra (L5)* (VL5=AT-1128+AT-2659+AT-6055). Complete L5 that only lacks the right transverse process.

Text S2. The determination of the Sima de los Huesos (SH) Pelvis 1 vertebrae and the vertebral formula of the SH hominins. The vertebral formula of our species is: 7 cervical, 12 thoracic, 5 lumbar and 5 sacral vertebrae (7/12/5/5) in 57.5% of the individuals, and 7/12/5/6 in 22.1% of the individuals in a sample of 181 individuals. Thus, five is the modal number of lumbar vertebrae present in our species, although other variants exist in a lower percentage (1). On the other hand, modern humans show greater variation in the number of coccygeal vertebrae, but the highest frequency in a sample of 109 individuals corresponds to a number of four (59.5%) and five (33.9 %) elements (1).

There is an ongoing debate regarding the evolution of the vertebral formula in the hominin lineage. All hominins show seven cervical vertebrae, which is the number of vertebrae for nearly all mammals. Based on different modern hominoid species as well as the fossil skeletons of *Australopithecus africanus* (Sts 14, Stw 431) and *Homo ergaster* (KNM-WT 15000), some authors propose the presence of 12 thoracic and six lumbar vertebrae in *Australopithecus* and early *Homo* (1-4) while others defend the existence of 12 thoracic and only five vertebrae in these species (5). Besides, it seems likely that four was the modal number of sacral vertebrae in these species (4).

Regarding *Homo neanderthalensis* only the partial skeleton of Kebara 2 preserves the entire vertebral column, and its vertebral formula is 7/12/5/5 (6). Although, not as complete as Kebara 2, other Neandertal individuals preserve substantial portions of their vertebral column (i.e., La Chapelle-aux-Saints, La Ferrassie 1, Régourdou 1, Shanidar 2, Shanidar 3). Although some of these individuals present anomalies in the vertebral column (7), most scholars do not question that the vertebral formula of Kebara 2 (7/12/5/5; i.e., that of our species) would be the modal for *Homo neanderthalensis* (7-10).

The SH Pelvis 1 individual preserves its last five presacral vertebrae and its sacrum is formed by six elements. Regarding the presacral vertebrae, all of them show lumbar characteristics: parasagittally oriented articular facets, absence of articular facets for ribs in the vertebral body, and presence of transverse processes.

With regard to the SH Pelvis 1 sacrum, S1 is completely sacral in form. The body of the S1 vertebra shows incomplete fusion to the second vertebral body and it shows a "second promontory" between these two vertebrae. This morphology of the S1-S2 junction is shared by all the other SH sacra that preserve the first two sacral vertebral bodies (AT-1005, AT-322 and AT-3711+AT-4200+AT-4350). On the other hand, the last and sixth element is conspicuously coccygeal in form when compared to modern humans and the morphology of the SH AT-6239 first coccygeal vertebra. Additionally, this last and sixth element's body shows incomplete fusion, both in the ventral and dorsal surfaces, to the fifth sacral vertebral body. The lateral transverse processes of the sixth sacral element are broken, so it is unknown if this element would have formed a sacral foramina. Besides, the SH AT-1005 sacrum shows only five sacral elements, showing the last one analogous shape to the fifth sacral element of SH Pelvis 1. It is therefore concluded that the sixth vertebral element represents the partially sacralized first coccygeal vertebra. In addition, the SH sample suggests that the caudal spine of the SH population was composed at least of three coccygeal elements: SH remains corresponding to the first (presence of cornua and transverse processes; SH AT-1570, AT-4308 and AT-6239), middle (two articular joints; AT-1830, AT-4306 and AT-6240), and the last or apical (one joint and one rounded apical extreme; AT-3853) vertebrae have been identified.

Until new evidence is found, our working hypothesis is that the vertebrae associated to Pelvis 1 represent the L1-L5 segment, the sacrum is composed of five sacral vertebrae and a partially fused first coccygeal vertebra. Thus, we propose the formula 7/12/5/5/≥3 as the modal vertebral formula for the Middle Pleistocene SH spine. This pattern, shared by Neandertals and modern humans, was likely present in the last common ancestor of the *H. neanderthalensis* and *H. sapiens.*

Text S3. Reconstruction of SH Pelvis 1. SH Pelvis 1 was recovered in six fragments during the 1994 Atapuerca field season: (*i*) AT-1000. Left ilium and ischium with the auricular surface perfectly preserved; (*ii*) AT-1000. Almost complete left pubis with limited or no physical contact either with the ilium or the ischium of the same side; (*iii*) and (*iv*) AT-1001. Right ilium and ischium plus a small fragment of the ischio-pubic ramus with no contact between them. The auricular surface is partially preserved and fractured; (*v*) AT-1002. Right pubis without actual articulation with the right ilium or ischium; (*vi*) AT-1003. Sacrum with intact auricular surfaces. None of these elements is affected by plastic deformation, and therefore no restitution process was needed. To avoid manipulation of the original fossil specimens, a high-resolution epoxy resin cast was used. The main concern of this new reconstruction was to minimize the asymmetries relative to the sagittal plane of the pelvis. This has been done by mirror imaging, as well as comparative anatomical criteria. The reconstruction was achieved in two steps: first, completing the regions of the six isolated fragments that do not determinate/participate in the reconstruction of the final pelvic ring shape, and second, articulating these fragments and completing the missing portions of the pelvic ring.

Reconstruction of the isolated fragments. *ASIS*. The area surrounding the ASIS is better preserved in SH Pelvis 1 than it is commonly seen in most human fossil hip bones. However, the most anterior-superior region of both iliac blades is affected by irregular breakages. Using as references two additional SH specimens (AT-1004+AT-1829+AT-6235 and AT-659+AT-3817) and the Kebara 2 pelvis, we have reconstructed the missing regions, including the anterior projection of the ASIS, following the curvature of the preserved portions of the anterior and anterior-superior margins of the iliac blade. *Sacro-iliac region*. This region is almost complete in the left os coxae; minor reconstruction was needed, preserving the anatomical consistency with the adjoining regions. The right os coxae was subsequently completed by mirror imaging of the left side. *Ischial spines*. This region is poorly preserved, even in modern osteological collections. The SH Pelvis 1 spines are broken close to their basal part, but they still preserve the distinctive inflection of the curvature in their caudalmost part. No other SH remain in the sample has better preserved ischial spines than Pelvis 1. In consequence, we have attempted a realistic reconstruction based on the present modern spine morphology, extending the caudal (in medial direction) and cranial (in caudo-medial direction) edges of the preserved portions of the SH Pelvis 1 ischial spines until they meet each other. *Some minor regions of the ossa coxae*. Lesser reconstruction was attempted based on anatomical consistency and mirror imaging in small regions of the right and left iliac crest and fossa, in the cortical bone of the left ischial tuberosity and inferior ischial ramus, and in the eroded right acetabular rim and left AIIS. *Sacrum and coccyx*. Major reconstruction of the lateral parts of the third, fourth and fifth sacral vertebrae has been attempted. This has been done by mirror imaging, and comparative anatomy from modern humans, and Kebara 2 and Shanidar 3 Neandertals. In addition, reconstruction of the promontory and the cranial portions of the medial crest was assessed by comparing the morphology of this individual and that of the AT-1005 specimen from SH. Besides, minor reconstruction was made on both sides, regarding the lateral crests and the sacral tuberosities. The partially sacralized first coccygeal vertebra was easily completed by mirror imaging of the right side. Their transverse processes have not been cranio-laterally extended up to join the caudal lateral portion of the fifth sacral vertebrae, although this could have been the case. Two additional caudal elements have been added to complete the coccyx. This has been roughly done scaling the morphology of three specimens from SH representing middle and apical coccygeal vertebrae (AT-1830, AT-4306 and AT-3853).

Reconstruction of the pelvic ring. The articulation of the six isolated elements and subsequent completion of the pelvic ring has been attempted by joining first those elements that fit better and show less movement. In consequence, we began by connecting the ilia to the sacrum, and then, closing the anterior wall of the true pelvis by articulating the pubic bones. (*i*) *Sacro-iliac joints*. The two major fragments representing the right (AT-1001) and left (AT-1000) ilia and ischia of SH Pelvis 1 can be directly articulated with the sacrum (AT-1003) along their sacro-iliac joint surfaces. Articulation of the left ischium and ilium (AT-1000) with the sacrum (AT-1003) was the first to be performed. The joint between these elements shows a better preservation and much more reduced mobility than the right one. A plastic surface simulating the anatomical sagittal plane was then attached along the middle of the ventral surface of the sacrum. The AT-1001 fragment was next articulated with the AT-1003 sacrum, at the position where the best overall symmetry and anatomical coherence relative to the left side was achieved. (*ii*) *Anterior wall of the true pelvis*. The two pubic bones (AT-1002 and AT-1000) and the right ischio-pubic ramus fragment (AT-1001) show none or limited contact with the other portions of their respective ossa coxae. The left pubis (AT-1000) was first connected to its side-corresponding ilium and ischium. This fragment preserves a small anterior portion of the lunate surface and the fossa of the acetabulum. Therefore, its position can be very precisely set taking into consideration several criteria: (*a*) the anatomical consistency of the ischiopubic ramus compared to that of another left male SH pubic bone (AT-2500+AT-4292+AT-6236) and the well-known modern male anatomy, (*b*) the sagittal position of the symphyseal surface, and (*c*) the dimensions and morphology of the acetabulum. Regarding the last criterion, the acetabulum can be reasonably well reconstructed considering (*1*) the shape of the lunate surface as a whole, and (*2*) the metrical relationship between the vertical and horizontal diameters (following ref. 11). The vertical diameter of the Pelvis 1 left acetabulum can be measured on the original (58.8 mm), but the horizontal dimension has to be estimated. We first considered the ratio between the horizontal/vertical acetabular diameters in two modern European male samples [Portuguese = 0.99 ± 0.35 (n = 202) and Medieval Spaniards = 0.94 ± 0.36 (n = 33)], in Kebara 2 (0.91) and in Krapina Cx.3+Cx.6 (0.92). Additionally, a regression line of the horizontal acetabular diameter (HAc) on the vertical one (VAc) was calculated for each recent human sample:

- European (Portuguese) HAc = 8.316 + 0.833 VAc (n = 202); r = 0.8
- European (Medieval Spaniards) HAc = 8.32 + 0.79 VAc (n = 33); r = 0.8

Considering both the ratios and the regressions, we obtain a horizontal acetabular mean range for Pelvis 1 at 53.5-57.9 mm. Finally, considering the other anatomical issues, we adopted 56 mm for the horizontal acetabular diameter of our Pelvis 1 reconstruction (horizontal/vertical acetabular diameter ratio = 0.95).

No compensation was made for the symphyseal cartilage. However, the somewhat ventral-facing symphyseal surfaces permit to attach a 3 mm-thick cartilaginous layer between the anterior parts of the pubic symphyses. This thickness is in agreement with observations on present populations (12).

After locating the left pubic bone, the right pubis (AT-1002) and the ischio-pubic ramus fragment (AT-1001) were subsequently articulated by mirror imaging relative to the left side. Finally, the complete restoration of the absent right superior pubic ramus was also performed through mirror imaging.

Text S4. Stature, body mass and encephalization quotient (EQ) calculation. In previous works (13, 14), we assigned two femoral fragments from SH (AT-432 and Femur X) to SH Pelvis 1. These remains were used to estimate the stature and body mass of this individual. However, Femur X was not a complete bone, and its maximum length (MFL) was estimated on the basis of the femoral head diameter (FHD) using a

general regression equation proposed by McHenry [MFL = FHD x 6.0642 + 155.3, r = 0.73 in ref. 15], and another one calculated by us from a European (Portuguese) sample of 70 modern male thighbones (MFL = FHD x 6.43 + 146.02; r = 0.65). According to these formulae, the MFL of Femur X was between 473 and 480 mm. We took 475 mm as the most likely value, also taking into account the relative position of various anatomical markers. This estimation assumes that the SH humans have similar joint proportions as recent humans. Fortunately, the SH sample has grown enormously and the missing portion of Femur X was recovered during the 2003 field season. The maximum length of Femur X measured directly on the now complete bone is 458 mm, almost 2 cm below our original estimate. Femur X presents a large femoral head relative to its length in comparison with various modern human means, thus leading to the overestimation of its length using the femoral head.
Moreover, one right and one left additional SH femora (Femur XII and XIII, MNI = 1), recovered from the SH site after the publication of Pelvis 1, could also be assigned to Pelvis 1 on the basis of anatomical congruency (large size and robusticity) between the femoral head and the acetabulum. Thus, from the lengths of these three femora (Femur X = 458 mm, Femur XII = 450 mm, Femur XIII = 450 mm), the single bi-iliac breadth of the revised reconstruction of Pelvis 1 (335 mm), and three different regression equations to estimate the stature (one modern multiracial and two white modern male equations from refs. 16-18), we have obtained an average stature range of 168.9-171.2 cm. From the uppermost and lowermost values of this range (168.9 and 171.2), and two modern male regression equations in refs. 19, 20, we have obtained a body mass range of 90.3-92.5 kg. The adult SH cranial capacity range is 1,100 (Cranium 5) – 1,380 (Cranium 4) cm^3 (ref. 21; p. 170). Using Martin's equation for the EQ (22) and relying on the upper- and lowermost values of the adult endocranial volume and body mass ranges, the resultant EQ is 3.1-3.2 based on Cranium 5 and 3.9-4.0 based on Cranium 4.

Text S5. Pelvic canal shape. ***Comments to Weaver and Hublin (23).*** *Regarding the shape of the outlet in modern populations*. As mentioned in the main text, our results show that the shape of the outlet is extremely variable both in modern males and females (*SI Appendix*, Fig. S4), contrary to the assertion that modern humans "typically have […] anteroposteriorly oval outlets" (ref. 23; p. 8151). *Regarding the primitive shape of the outlet in hominins.* Weaver and Hublin proposed that a transversely oval outlet appears to be the primitive shape in hominins (23). However, the outlet shape in modern humans is quite variable, and the SH Pelvis 1 and (probably) Gona pelvis are not significantly different from modern humans in their outlet index values (*SI Appendix*, Fig. S5). Therefore, our results on these individuals do not support the conclusion of these authors. ***Additional Pelvic Remains.*** *Jinniushan (China).* The female left hip-bone from Jinniushan (Middle Pleistocene, China) has been argued to represent the archaic condition in *Homo* (24). Rosenberg and coworkers attempted to reconstruct the pelvic inlet shape and bi-iliac breadth, obtaining a pronounced oval inlet shape (Inlet index = 73%) (25). Although, they did not deal with the shapes at the midplane and outlet, mirror imaging of Figure 2 of their work yields a reconstruction of the pelvis in superior view that clearly shows mediolaterally (M-L) marked oval midplane morphology (25). In our opinion, this tentative and limited evidence agrees with the pattern of sexual dimorphism described in the present study with archaic *Homo* females, like Jinniushan, showing more platypelloid midplanes than in the male SH Pelvis 1. *Kebara 2 (Israel).* Tague notes that the male Neandertal pelvis from Kebara 2 shows a notably low index of pelvic funnelling (outlet circumference x 100/inlet circumference) relative to modern males (26). Our study on the original Kebara 2 material shows a remarkable crushing in anterior-posterior direction of the whole sacrum that results in an anomalous flat and straight morphology that differs from the typical curvature of modern humans, SH Pelvis 1 and Shanidar 3 sacra. Among other consequences, this has probably modified the actual sagittal dimensions of the pelvic canal. Therefore, this specimen has not been considered when analysing the morphology of the bony pelvic canal in the present study. *Ponce de Leon and coworkers' reconstruction of Tabun C1 (Israel) (27).* The birth canal reconstruction of the Tabun C1 Neandertal done by Ponce de Leon *et al.* (27) clearly differs from that of Weaver and Hublin (23). In their Tabun C1 reconstruction, Ponce de Leon and colleagues assumed (without justifying) a modern human-like birth passage in Neandertals (i.e., rotational birth) and subsequently considered that the A-P outlet dimensions were constrained by the maximum length of the Mezmaiskaya skull (27). This assumption precludes including this reconstruction when dealing with the shape of the pelvic canal in the present study (also noted by ref. 23). On the other hand, Weaver and Hublin performed the Tabun C1 pelvis reconstruction from the preserved fossil portions of this specimen alone (23).

Text S6. Measuring methods of the anatomical parameters involved in the sagittal spino-pelvic balance. ***Sacral anatomical orientation (SAO)*** (*SI Appendix*, Fig. S6A). *Definition*: this angle was defined by Peleg and coworkers (28), with the goal of introducing a new technique to define the sacrum orientation in skeletal material. It assumes that the two ASIS and the pubic crest are located in the same coronal plane when in normal anatomical position. The SAO is the angle between the intersection of the line running from the most anterior and posterior midsagittal points of the sacral plate, and the plane running from the two ASIS and the anterior-superior border of the pubic symphysis. *Measuring method*: Mimics 13.0 software (Materialise) was used to carry out the 3D CT reconstruction of Pelvis 1 and, subsequently, the registration of the landmark coordinates. Using a geometrical technique akin to that of Peleg and coworkers (28), we first registered the three points that define the previously mentioned coronal plane [i.e., the two ASIS (a, a'), and the most anterior-superior point of the border of the pubic symphysis (b)]. Next, we registered the most anterior [i.e., sacral promontory (c)] and most posterior (d) points of the sacral plate in the midsagittal plane. Due to the slightly fragmentary state of the promontory and to the "dome-shaped" sacral plate of Pelvis 1 (29), two different measures of the SAO angle were calculated based on two different landmarks at the anterior part of the sacral plate: (*i*) the one in the preserved portion of the fossil that more closely resembles the actual position of the promontory, and (*ii*) the one resulting from minor reconstruction of the promontory. The angle between the intersection of the coronal plane and the sacral line (SAO,α) is also the angle between the normal vector of the plane ($\bar{n}$) and the direction vector of the line ($\bar{b}$). Once the coordinates of these vectors are calculated (using the landmark coordinates), the SAO is obtained as follows:

$$SAO(^{\circ}) = \arcsin \frac{\bar{n} \cdot \bar{b}}{|\bar{n}| \cdot |\bar{b}|}$$

Pelvic incidence (PI) (*SI Appendix*, Fig. S6A). *Definition*: this angle was originally defined on the basis of X-ray images by Duval-Beaupère and collegues as the angle between the line perpendicular to the sacral plate at its midpoint and the line connecting this point to the center of the bicoxo-femoral axis (30). More recently, Peleg and coworkers have developed a method to measure it in skeletal material, replacing the axis of the femoral head for the biacetabular axis (28). *Measuring method*: PI was measured in SH Pelvis 1 and Pelvis 2. This was done by means of Mimics 13.0 software (Materialise), using a 3D CT reconstruction (Pelvis 1) and a surface scan (Pelvis 2), from which registration of the landmark coordinates were recorded. Four points were registered: first, two at the deepest (most medial) part of each acetabular fossa, defining the acetabular axis that determines the axis midpoint (M). Second, two at the most anterior (c) and posterior (d) points of the sacral plate in the sagittal plane. These two latter points were also used to calculate the midpoint (center) of the sacral plate (O). Note that, as in the SAO calculation, two different landmarks were considered at the anterior sacral plate margin when calculating the PI value of Pelvis 1: (*i*) the one obtained without reconstruction of the small damaged portion of the sacral promontory, and (*ii*) that obtained on the reconstruction. Subsequently, PI (β) was defined as the angle between the line connecting the midpoints of the acetabular axis (O) and the sacral plate (M), and that defined by the points (c) and (d). This was done by means of the cosine of the angle (θ) between two vectors (for detailed mathematical formulation see ref. 28; p. 972):

$$PI(^{\circ}) = 90 - \arccos\theta$$

where,

$$\cos\theta = \cos\alpha_{MO} \cdot \cos\alpha_{cd} + \cos\beta_{MO} \cdot \cos\beta_{cd} + \cos\gamma_{MO} \cdot \cos\gamma_{cd}$$

Vertebral wedging (*SI Appendix*, Fig. S6B). *Definition*: we have followed the definition in ref. 31 to calculate the vertebral wedging angle from the formula:

$$Vertebral\ wedging(^{\circ}) = 2 \arctan (Y/X)$$

where,

X = Anteroposterior height

Y = (Posterior height – Anterior height)/2

The *SI Appendix*, Table S6 shows the "anteroposterior height" as the "cranial dorsoventral diameter" (M4 from Martin's number in ref. 32), whereas the "posterior and anterior heights" are respectively referenced as the "dorsal" and "ventral cranio-caudal diameters" (M2 and M1 from Martin's number in ref. 32, respectively). *Measuring method*: direct measurements were taken with standard sliding callipers (0.1 mm precision) on the bones/fossils.

Text S7. CT and surface scan information. A 3D CT reconstruction of the articulated Pelvis 1 using Mimics 13.0 software (Materialise) were performed (CT-scan parameters: 0.5 mm slice increment, 160 kV, 4 mA, 1,024 x 1,024 matrix, 0.29291016 mm pixel size). Additionally, a 3D surface scan of the articulated Pelvis 1 was achieved (Konica Minolta 3D Laser Scanner VI-9i; Precision: 0.25 mm, Resolution: 640 x 480 pixels). We also performed a CT-scan of the original Pelvis 1 sacrum (AT-1003) (CT-scan parameters: 0.2 mm slice increment, 160 kV, 4 mA, 1,024 x 1,024 matrix, 0.18081227 mm pixel size). In addition, a 3D surface scan of the SH Pelvis 2 was done (Next Engine Desktop 3D Scanner, Precision: 0.38 mm, Resolution: 75 dpi). Finally, we also made a 3D CT reconstruction (Mimics 13.0 software, Materialise) of a male medieval human coming from the Sepulveda Church Collection from Segovia, Spain (CT-scan parameters: 0.5 mm slice increment, 160 kV, 4 mA, 1,024 x 1,024 matrix, 0.29291016 mm pixel size).

Supporting Information II: Figures

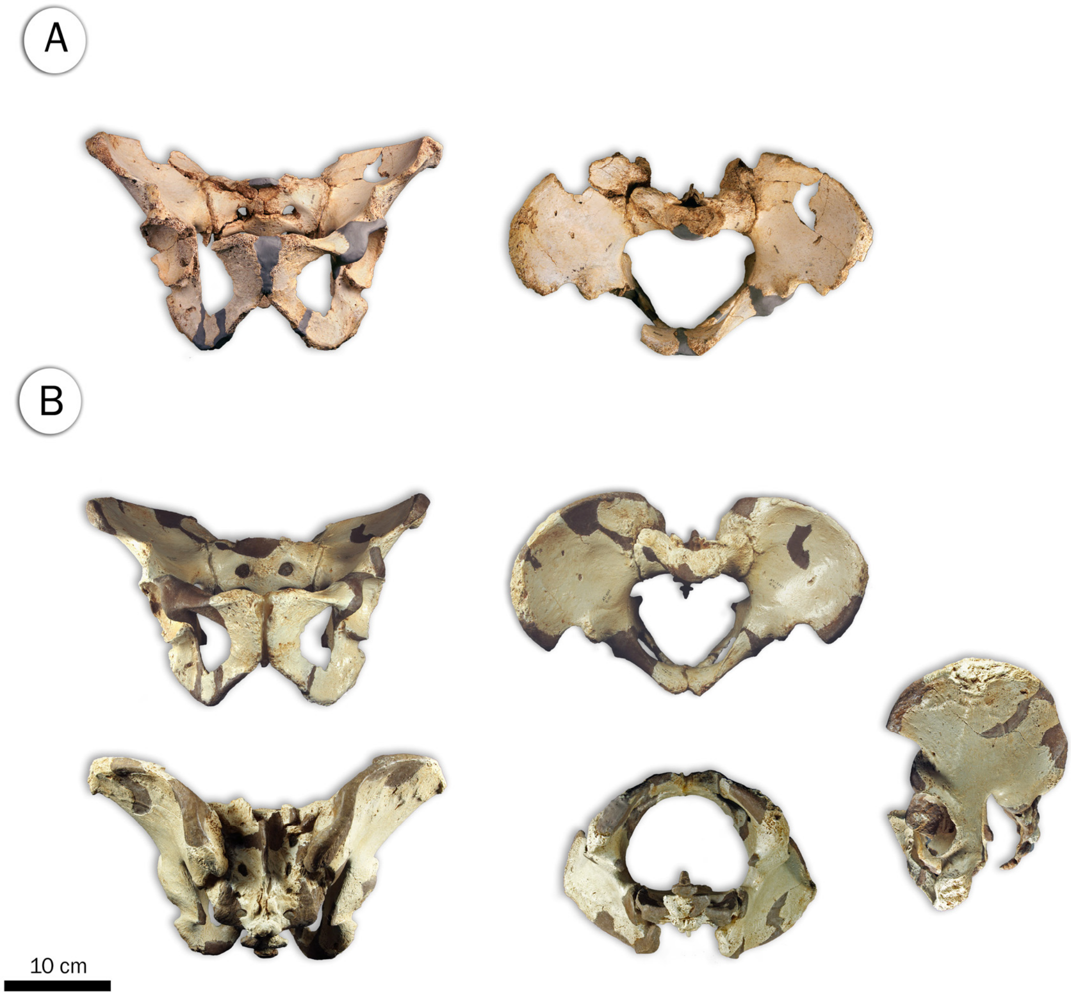

Figure S1. Reconstruction of SH Pelvis 1 according to (*A*) ref. 13 in anterior (*Left*) and superior (*Right*) views, compared to (*B*) that from the present study in anterior, posterior, superior, inferior and lateral views (from *Top* to *Bottom*, and *Left* to *Right*).

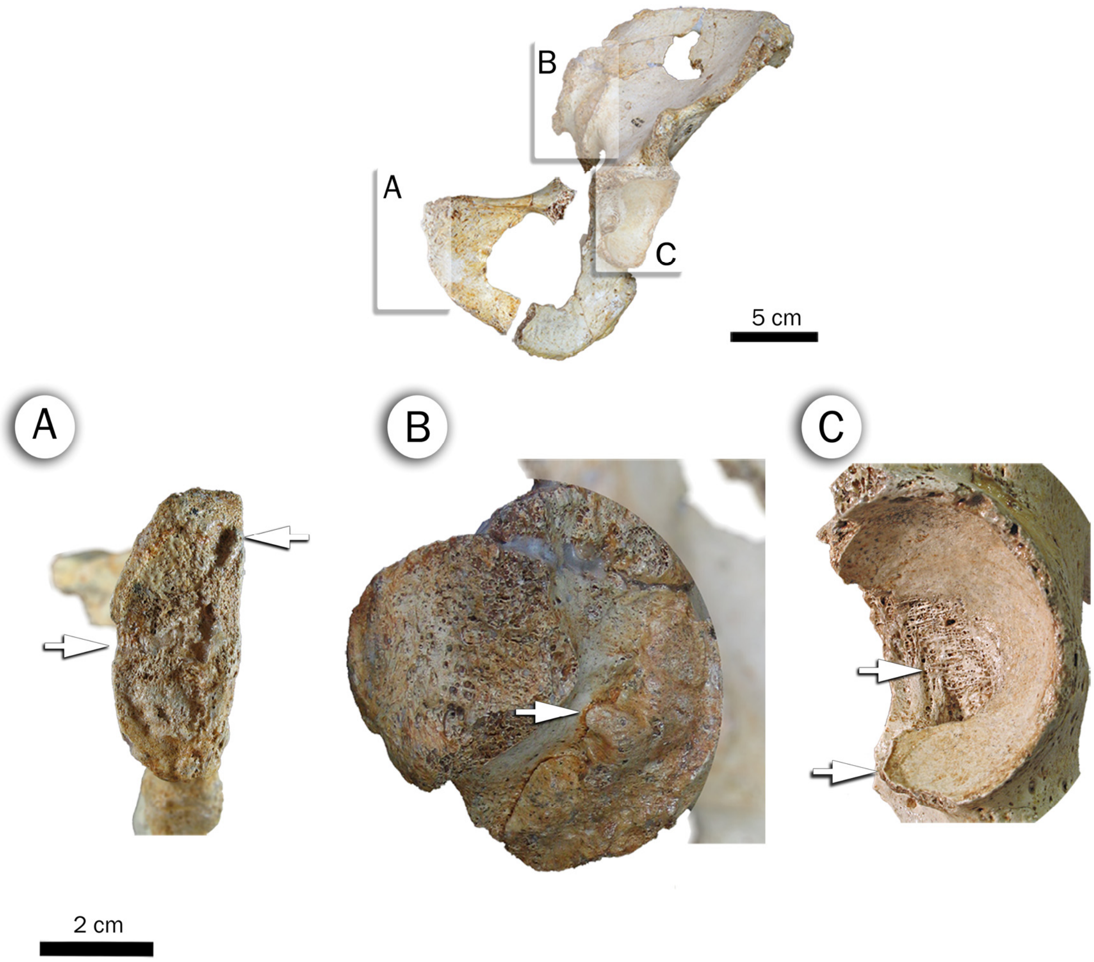

Figure S2. State of the characters used to assess the developmental stage and age-at-death of the SH Pelvis 1 individual: (*A*) Pubic symphysis showing mostly eroded rim, partial destruction and lipping at the dorsal margin (*Left* arrow), and some pitting on the symphyseal surface (*Right* arrow). (*B*) Auricular surface showing the absence of billowing and advanced formation of dense bone (arrow). (*C*) Acetabulum. The fossa is deep and intensively covered with micro- and macroporosity (upper arrow) and the lunate surface shows pronounced osteophytic activity at the apex (lower arrow).

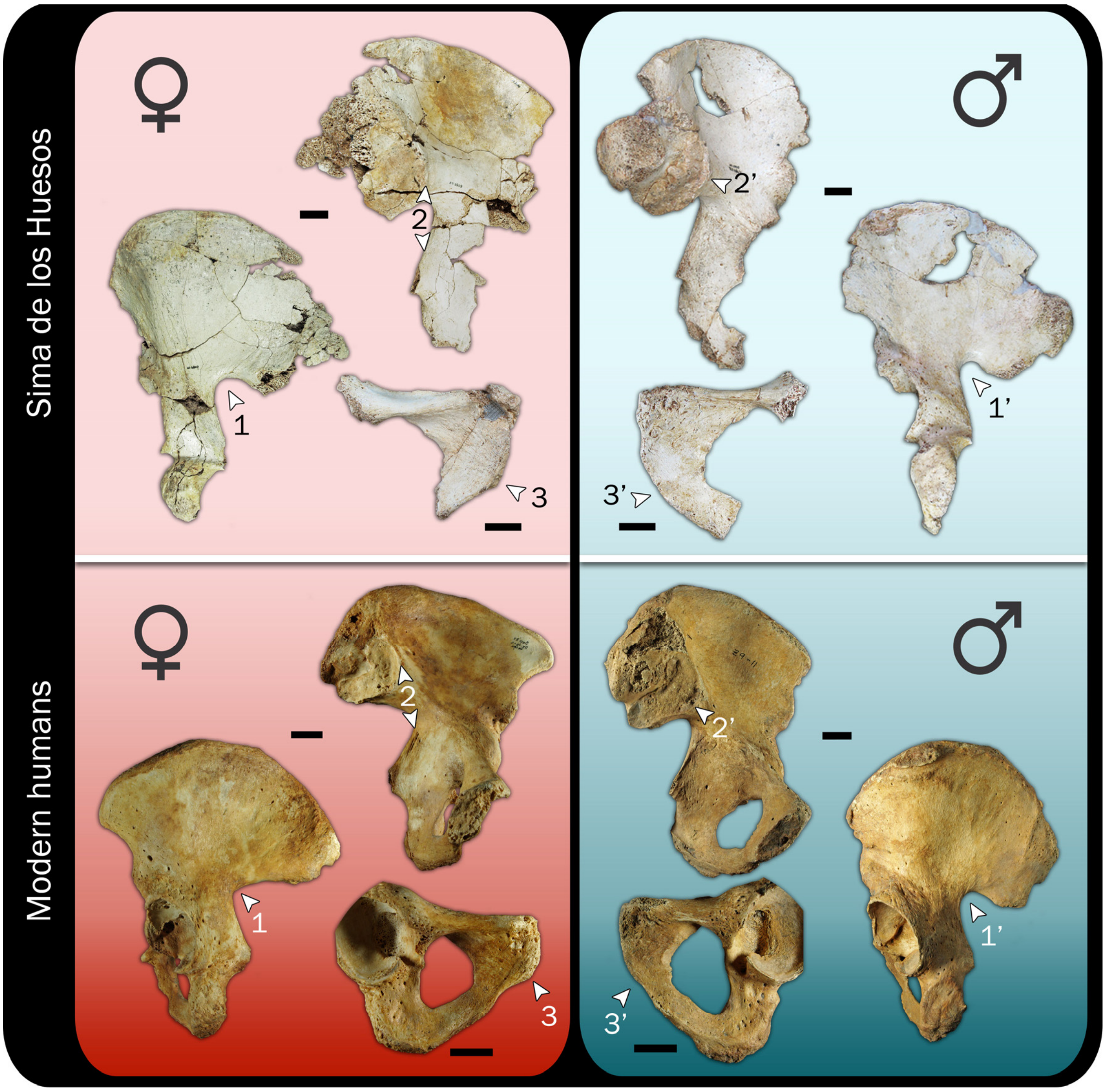

Figure S3. Intrapopulation variation and sexual dimorphism within the SH pelvic sample. Modern dimorphic traits are related to the fossil variation of the SH sample: (1-1') Greater sciatic notch aperture; (2-2') Composite arch (presence/absence); (3-3') Development of the subpubic concavity and ventral rampart, subpubic angle, and shape of the pubic body. Note that although differences between SH female-like and male-like morphologies are conspicuous (mainly between the 1-1' and 3-3' character states), they are not as remarkable as between sexes in modern humans. SH material: ♀ = Coxal III (ilium + ischium) and AT-1006 (pubis); ♂ = AT-1000 (SH Pelvis 1). Scale bars = 2 cm.

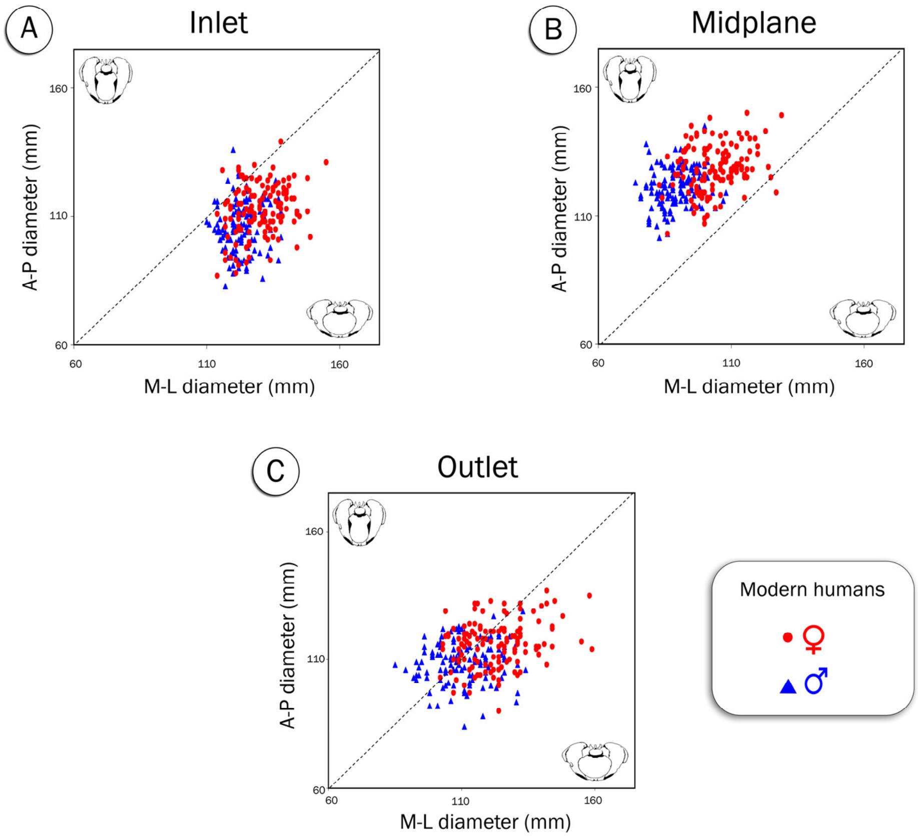

Figure S4. Modern pelvic canal shape defined from bivariate plots of the sagittal (A-P) to the transverse (M-L) diameters in the (*A*) inlet, (*B*) midplane and (*C*) outlet. Dashed lines separating oval transverse shapes (*Bottom Right* corner) from oval sagittal shapes (*Top Left* corner). Despite morphological similarities between females and males for all planes (inlet: M-L oval shape; midplane: A-P oval shape; outlet: variable for both sexes), females show significantly more pronounced transverse oval shapes than males in the midplane and outlet (*t* test; $P < 0.0001$ and $P < 0.001$, respectively). Definition of the sagittal and transverse diameters from ref. 26. Data from one European (Portuguese) sample [*n* (♂) = 125; *n* (♀) = 130].

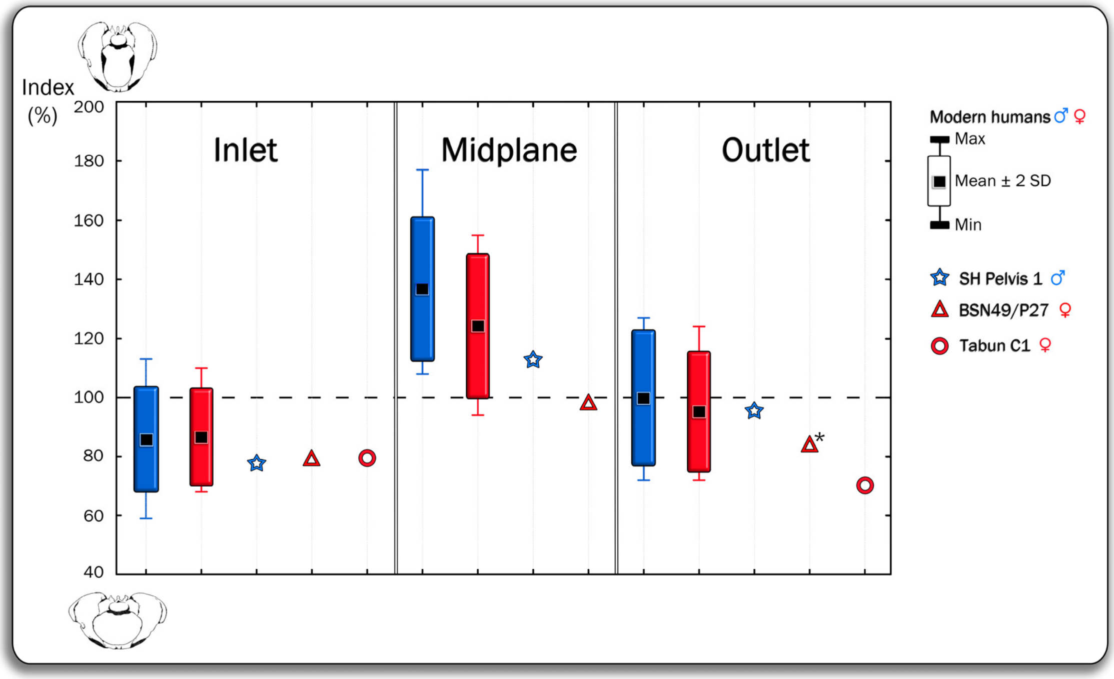

Figure S5. Inlet, midplane and outlet indices for three pelvic fossils and the modern comparative sample. All indices calculated from (sagittal/transverse diameters) x 100 in the inlet, midplane and outlet. Definition of sagittal and transverse diameters from ref. 26. Dashed line separating sagittal oval shapes (index > 100%) from transverse oval shapes (index < 100%) of the pelvic canal. Modern data from a European (Portuguese) sample [*n* (males) = 125; *n* (females) = 130]. The midplane index value of SH Pelvis 1 is calculated from the reconstruction of its ischial spines. The value of the SH Pelvis 1 midplane index without reconstruction of its spines is also > 100% (i.e., sagittal oval shape) (see *SI Appendix,* Table S2). Tabun C1 and BSN49/P27 data from refs. 23, 33, except (*) representing maximum outlet index of BSN49/P27 calculated using the value of its sacral midplane diameter as the highest value for its sagittal outlet diameter [sagittal midplane diameter > sagittal outlet diameter in 94.5% of the individuals in the European (Portuguese) modern sample (*n* = 255)].

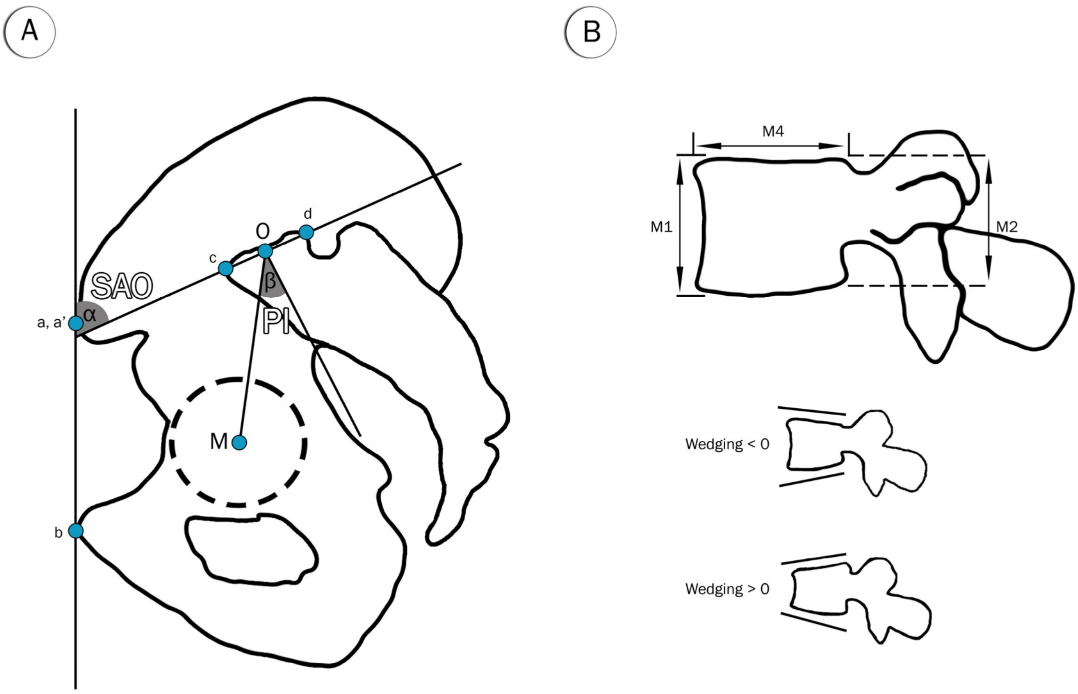

Figure S6. Calculation of the (*A*) sacral anatomical orientation (SAO, α), pelvic incidence (PI, β) and (*B*) vertebral wedging angles. See *SI Appendix*, Text S6 for detailed definition of landmarks and variables.

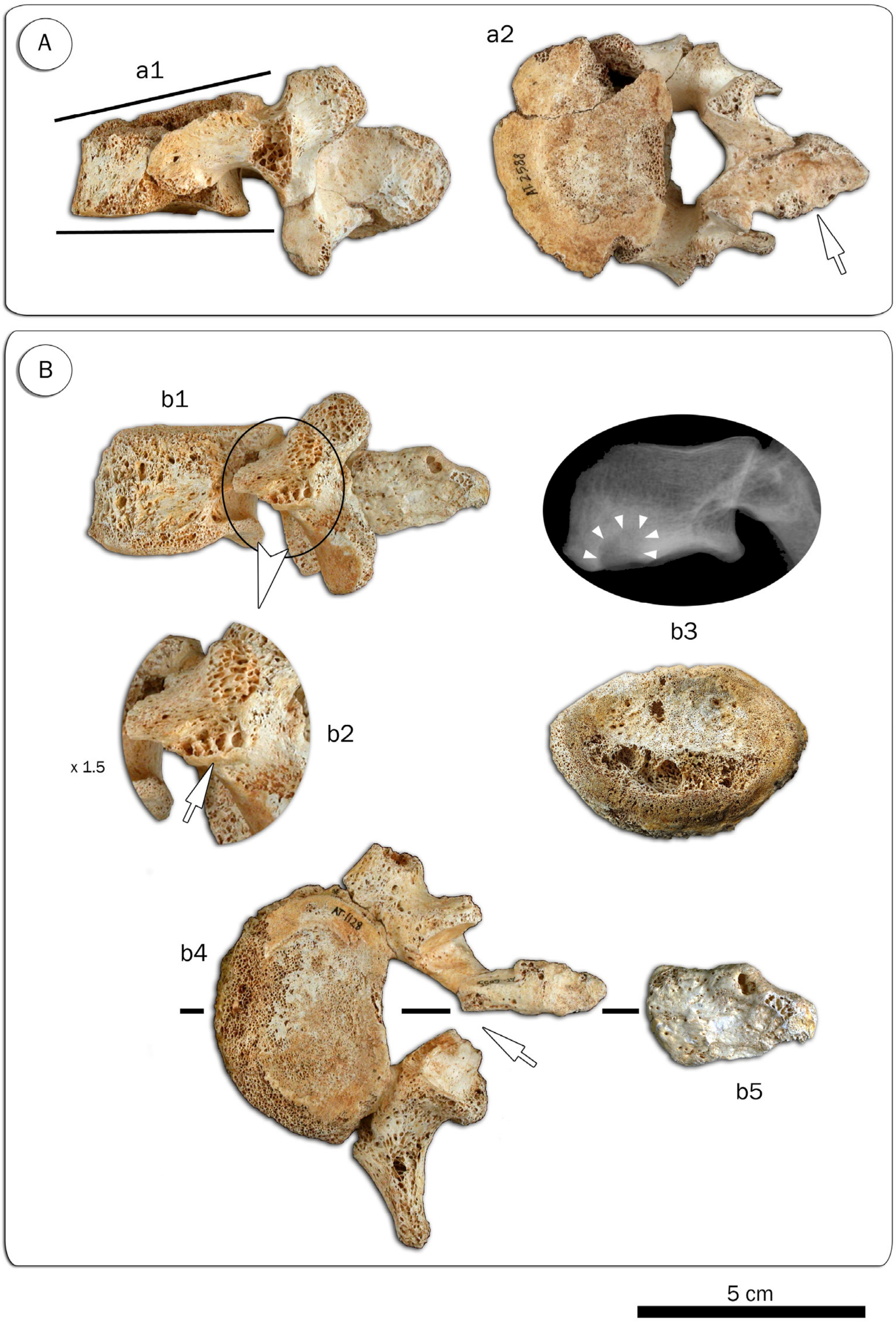

Figure S7. Pathological signs of L4 and L5 vertebrae of the SH Pelvis 1 individual. (*A*) Left lateral (a1) and caudal (a2) views of L4, showing its extreme ventral wedging and the extensive remodelling of its spinous process (arrow). (*B*) L5 vertebra. Its left lateral view shows the conspicuous remodelling of the body (b1) and the additional articular facet under the left pedicle (b2). The very large lytic lesion and the peripheral reaction (white triangles) are depicted in the lateral X-ray image (*Top*) and in the caudal view of the original (*Bottom*) (b3). Note the position of its spinous process relative to the midsagittal plane and the absent left lamina (arrow), in caudal view (b4). The left surface of its spinous process surface does not show sutures or fractures to the lamina (b5).

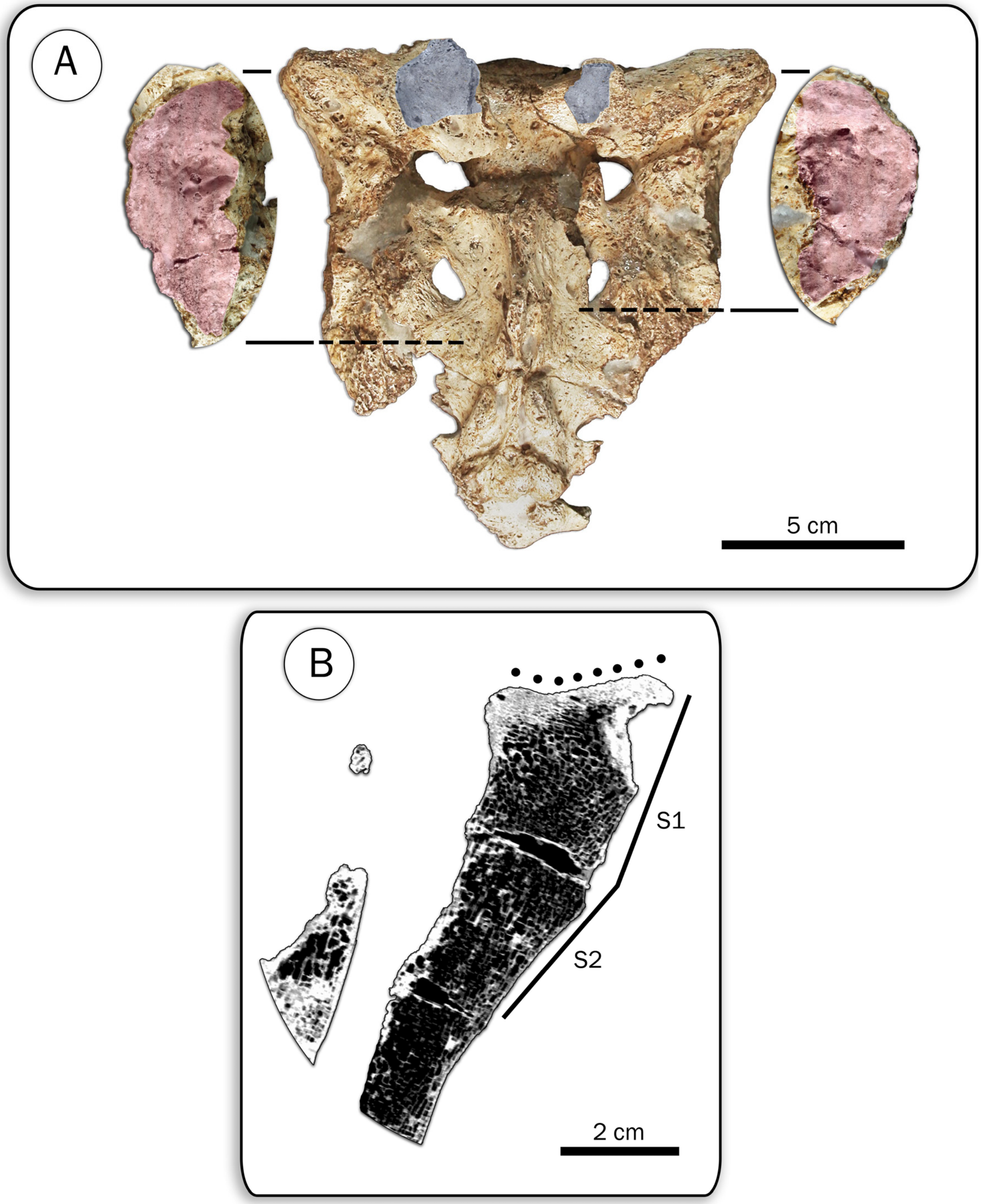

Figure S8. Sacrum of SH Pelvis 1 (AT-1003). (*A*) Differences in shape and size between the left and right auricular surfaces (in purple) and superior articular processes (in gray). (*B*) Midsagittal CT scan image showing the dome-shaped sacral plate (dotted line) and the dorsal rotation of the first sacral body (S1) relative to the body of the second vertebra (S2) (solid lines), that results in a "second promontory".

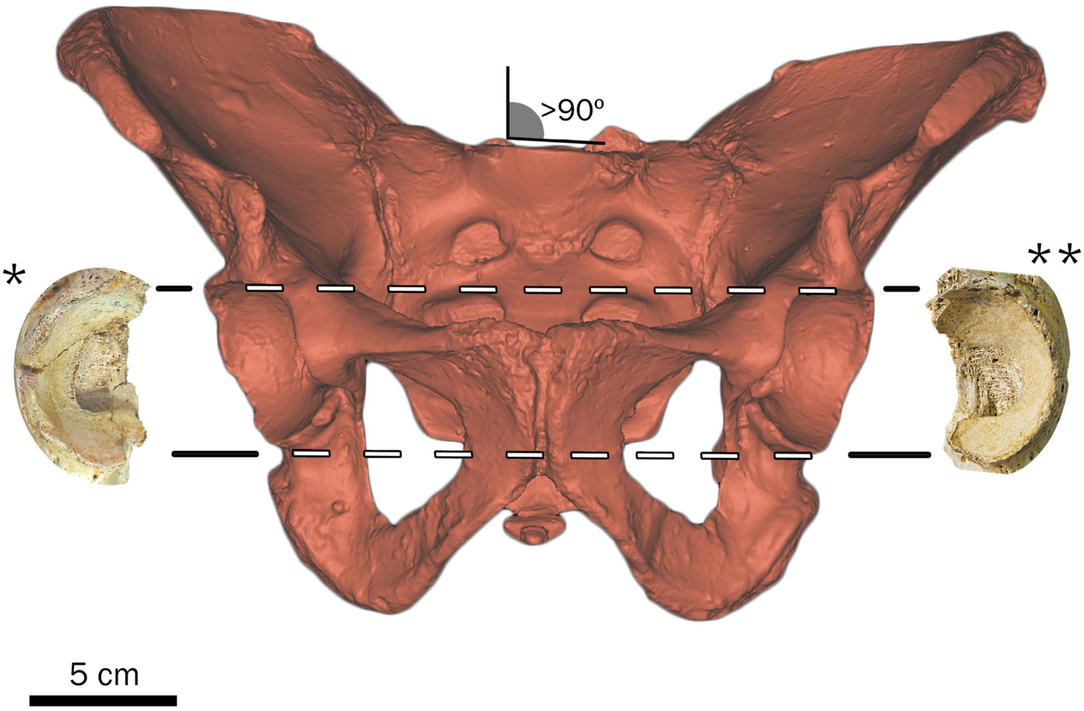

Figure S9. Anterior view of Pelvis 1 (surface scan rendering), showing the nonparallel orientation of the biacetabular axis (horizontal, dashed lines) and the sacral plate (left tilted, solid line). In addition, the right (*) and left (**) acetabuli demonstrate similar osteophytic formation in the iliac part of the acetabular rim, coupled with micro and macroporosity in the dorsal half part of the acetabular fossa.

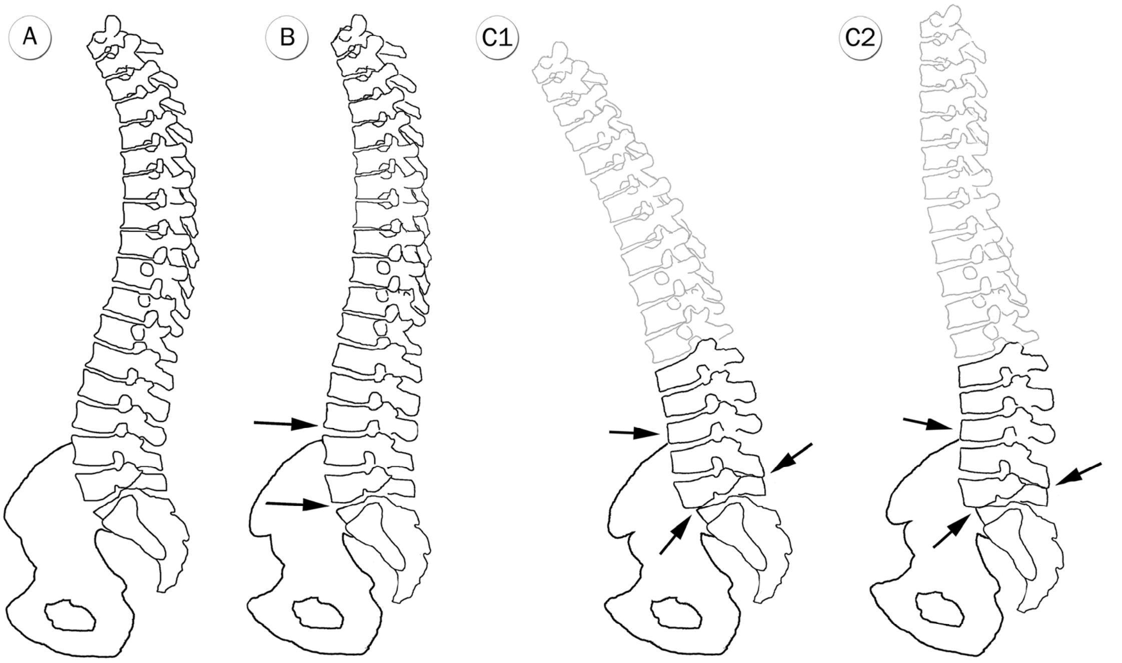

Figure S10. A schematic view of the sagittal thoracic, lumbar and pelvic configurations proposed in this study: (*A*) modern *Homo sapiens*. (*B*) Neandertal lineage [kyphotic vertebral bodies in L1-L4 (hypolordotic spine) (upper arrow); more horizontally oriented sacral plate (lower arrow)]. (*C*) SH Pelvis 1 individual depicted both without (*C1*) and with (*C2*) compensatory mechanisms, following refs. 34-36 [arrows from *Top* to *Bottom*: extremely kyphotic vertebral bodies in L2-L4; Baastrup disease in L4-L5; spondylolisthesis between L5 and S1].

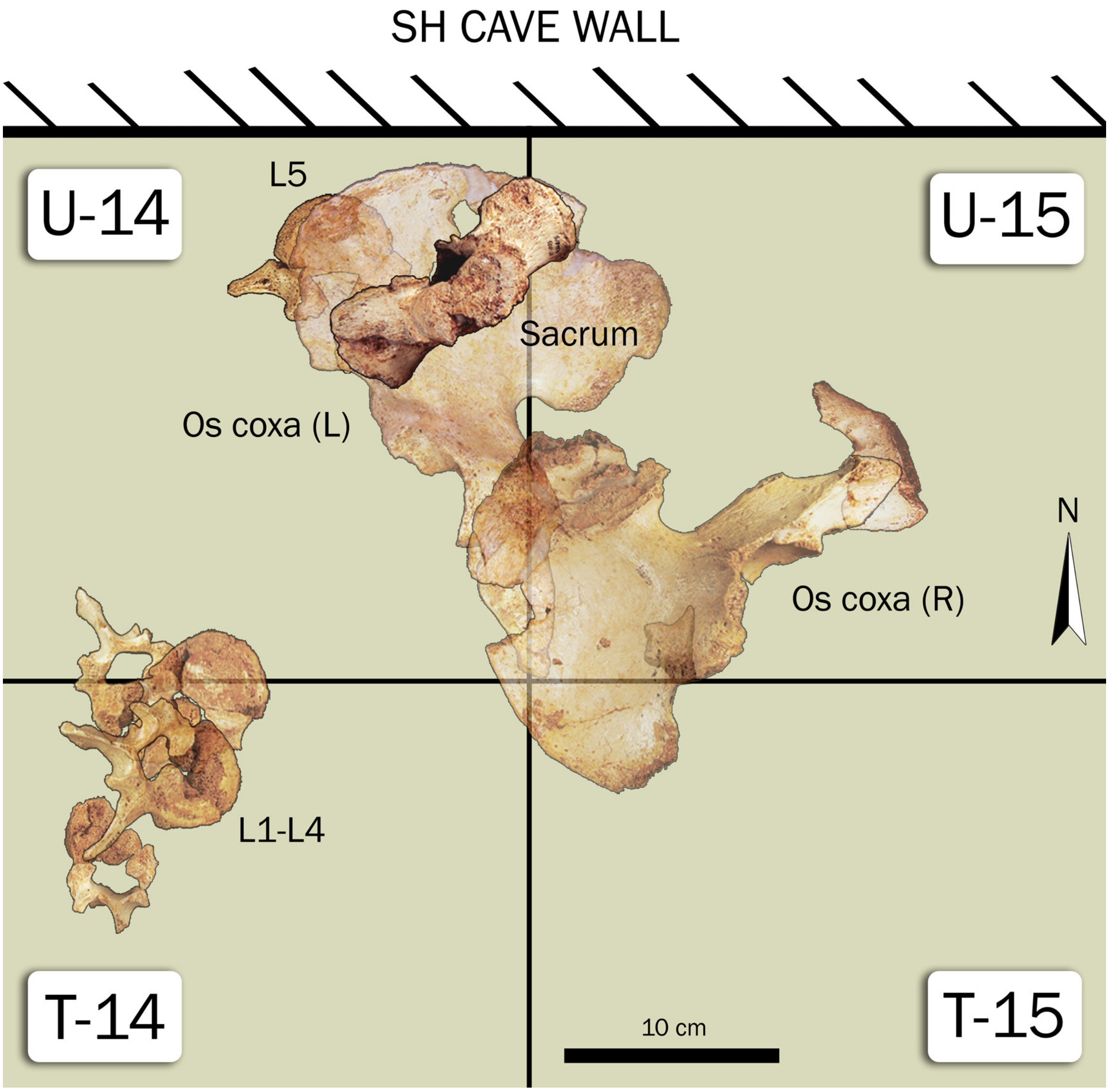

Figure S11. In situ reconstruction (plan) of the elements composing the SH Pelvis 1 individual. The first (L1) to fourth (L4) lumbar vertebrae arrangement is schematic and based on numerous fragments found around the figured area. The cave wall position corresponds approximattely to the the level where the pelvic bones and the fifth lumbar vertebra were found. T/U-14/15 = 0.5m-side squares of the SH excavation grid.

Supporting Information III: Tables

Table S1. Inventory of the SH Pelvis 1 individual

<table>
<tr><th>Region</th><th colspan="2">Specimen*</th><th>Description</th><th>Material</th></tr>
<tr><td rowspan="5">Lumbar spine</td><td colspan="2">[VL16(L1) = AT-2592+AT-2695+AT-2707+AT-4038+AT-4906][c]</td><td>Fragmentary first lumbar vertebra (L1)</td><td rowspan="5">Original + X-ray imaging (L5)</td></tr>
<tr><td colspan="2">[VL1(L2) = AT-2590+AT-2593+AT-2693+AT-2705+AT-2706][c]</td><td>Fragmentary second lumbar vertebra (L2)</td></tr>
<tr><td colspan="2">[VL2(L3) = AT-2589+AT-2591+AT-2594+AT-2657][c]</td><td>Complete third lumbar vertebra (L3)</td></tr>
<tr><td colspan="2">[VL3(L4) = AT-2588+AT-2658][c]</td><td>Complete fourth lumbar vertebra (L4)</td></tr>
<tr><td colspan="2">[VL5(L5) = AT-1128+AT-2659+AT-6055][c]</td><td>Complete fifth lumbar vertebra (L5)</td></tr>
<tr><td rowspan="3">Pelvis</td><td rowspan="3">Pelvis 1[b] =</td><td>AT-1000[a,b]</td><td>Complete left os coxae in two fragments: 1) ilium+ischium; 2) pubis</td><td rowspan="3">Original + cast + computer tomography (CT) scan + surface scan</td></tr>
<tr><td>(AT-1001+AT-1002)[b]</td><td>Almost complete right os coxae in three fragments: 1) ilium + ischium (AT-1001); 2) ischio-pubic ramus fragment (AT-1001); 3) pubis (AT-1002)</td></tr>
<tr><td>AT-1003[a,b]</td><td>Almost complete sacrum and first coccygeal vertebra</td></tr>
</table>

* (a) Previously published in refs. 37, 38.
(b) Previously published in ref. 13.
(c) Previously referenced in ref. 39.

Table S2. Comparative pelvimetry of the SH Pelvis 1 individual

Region	Variable§	SH Pelvis 1 individual		Male Z- score	Female Z- score	Modern Males¶	Modern Females¶
		ref. 10	**Present Study**			*Mean ± SD (range)(n)*	*Mean ± SD (range)(n)*
Os coxae‖	Maximum coxal height	240	240.0	3.0**	4.7**	211.9 ± 9.3 (189.0/238.0)(208)	196.3 ± 9.4 (166.0/219.0)(182)
	Iliac height	-	140.8	2.7**	3.3**	124.1 ± 6.2 (104.0/143.6)(208)	118.7 ± 6.7 (97.8/141.0)(176)
	Maximum iliac breadth	-	(180.8)	3.2**	3.6**	155.6 ± 7.9 (136.5/185.0)(192)	152.9 ± 7.9 (130.0/174.0)(165)
	Lower iliac height	(57)	(59.2)	0.4	-0.3	56.8 ± 5.5 (41.0/75.0)(210)	61.1 ± 6.3 (45.8/79.5)(179)
	Supraacetabular-Ilioauricular diameter	-	76.5	1.7	1.1	68.1 ± 5.0 (57.4/82.9)(220)	69.7 ± 6.0 (55.2/87.0)(186)
	Minimum iliac breadth	-	61.4	0.2	1.9	60.8 ± 3.8 (51.6/69.7)(221)	54.8 ± 3.4 (46.7/65)(187)
	Pubic length	(102)	(98.8)	2.2*	1.9	86.4 ± 5.6 (68.1/99.6)(187)	87.9 ± 5.8 (71.0/102.5)(167)
	Nonarticular pubic length	82	(83.9)	4.1**	3.3**	66.9 ± 4.2 (54.6/79)(188)	69.5 ± 4.4 (56.9/81.0)(166)
	Superior pubic ramus depth	-	10.7	-1.9	-1.5	15.3 ± 2.4 (9.3/22.9)(212)	13.8 ± 2.1 (8.8/18.4)(184)
	Ischial length	105.5	105.5	0.7	3.2**	94.5 ± 4.8 (79.6/112.0)(200)	84.9 ± 4.2 (72.0/94.0)(155)
	Vertical acetabular diameter	60	58.8	1.3	3.3**	55.2 ± 2.8 (48.2/62.0)(213)	49.9 ± 2.7 (41.7/60.5)(186)
	Ischio-pubic index‡	96.7	100.9	2.0*	-0.5	91.7 ± 4.7 (70.2/107.8)(175)	103.8 ± 5.4 (90.2/117.1)(138)
Sacrum	Sacral breadth	111.1	111.1	-0.4	-0.3	113.6 ± 6.1 (100.9/132.9)(72)	113.3 ± 7.2 (93.6/130.1)(75)
	Sacral lenght, straight††	-	116.1	0.1	0.8	114.6 ± 11.3 (89.6/137.3)(72)	108.4 ± 10.0 (77.7/133.6)(75)
	Sacral lenght, curved††	-	120.7	0.8	-	114.0 ± 8.0 (268)	-
	Sagittal sacro-lumbar plate diameter	-	(31.4)	0.1	1.3	31.2 ± 2.6 (25.9/38.0)(72)	28.4 ± 2.3 (17.7/33.5)(72)
	Maximum transverse sacro-lumbar plate diameter	-	52.3	0.4	1.7	50.2 ± 5.3 (39.1/61.1)(72)	44.8 ± 4.5 (34.1/56/1)(75)
	Angulation of the sacrum	-	46.0	-3.4**	-	62.3 ± 4.9 (345)	-
Pelvis	Maximum pelvic breadth (bicrestal breadth)	340	335.0	5.5**	3.3**	261.7 ± 13.3 (232/299)(125)	260.8 ± 22.4 (120/306)(130)
	AIIS-AIIS diameter	-	196.8	0.8	0.8	186.8 ± 12.0 (130/220)(125)	186.6 ± 12.0 (137/213)(130)
	ASIS-ASIS diameter	-	(271.9)	3.3**	2.5*	225.7 ± 14.0 (184/260)(125)	225.5 ± 18.7 (140/267)(130)
	PSIS-PSIS diameter	-	(71.8)	0.6	-0.2	67.7 ± 7.0 (50/85)(125)	73.2 ± 9.3 (52/101)(130)
	PIIS-PIIS diameter	-	(111.5)	4.7**	3.7**	87.5 ± 5.1 (75/102)(125)	88.1 ± 6.4 (72/109)(130)
	Transverse inlet diameter	138	139.3	2.0*	1.1	123.5 ± 7.8 (110/180)(125)	130.4 ± 8.4 (114/155)(130)
	Minimum biacetabular breadth	133.5	134.9	4.0**	2.6**	109.2 ± 6.4 (96/127)(124)	114.6 ± 7.9 (96/135)(128)
	Transverse midplane diameter (bispinal breadth)	(108)	(125.1-116.4)†	3.9**	1.3	89.0 ± 7.0 (74/108)(125)	103.8 ± 9.4 (83/129)(130)
	Transverse outlet diameter (bituberous breadth)	135	133.6	2.2*	0.9	110.2 ± 10.7 (85/134)(125)	122.9 ± 12.1 (102/159)(130)
	Maximum transverse diameter of the midplane	121	127.0	3.8**	1.4	99.5 ± 7.2 (86/116)(125)	112.0 ± 10.8 (88/177)(130)
	Sagittal external diameter	-	(176.3)	1.8	1.2	159.9 ± 9.4 (140/189)(124)	162.5 ± 11.6 (133/195)(130)
	Sagittal Inlet	109.4	(108.3)	0.9	0.1	99.5 ± 9.9 (73/134)(125)	107.7 ± 9.6 (84/130)(130)
	Sagittal midplane diameter	133	131.2	1.4	0.4	121.1 ± 7.4 (101.5/145)(125)	127.9 ± 9.2 (103/150)(130)
	Sagittal outlet diameter	126.5	127.5	2.3*	1.3	109.2 ± 8.1 (84/129)(123)	116.1 ± 9.0 (90/137)(129)
	Circumference inlet	405	405.7	1.5	-	370.0 ± 24.0 (234)	-
	Circumference midplane	347	(353.2-343.0)†	3.1**	-	297.0 ± 15.0 (89)	-
	Circumference outlet	395	412.4	4.7**	-	324.0 ± 19.0 (193)	-
	Subpubic angle	76	76.0	1.1	-0.4	66.8 ± 8.7 (43/90)(125)	79.4 ± 8.3 (61/97)(91)
	Divergence angle of the iliac blades	134	116.0	1.9	1.6	98.7 ± 9.3 (78/123)(124)	99.2 ± 10.3 (78/126)(91)

Measurements given in milimeters and sexagesimal degrees. Estimations in parentheses.

Z-scores calculated from the values of the present study Pelvis 1 reconstruction.

Male Z-score = (Fossil value - Modern male mean) / Modern male SD ; Female Z-score = (Fossil value - Modern female mean) / Modern female SD

(AIIS) Anterior inferior iliac spine; (ASIS) Anterior superior iliac spine; (PSIS) Posterior superior iliac spine; (PIIS) Posterior inferior iliac spine; (SD) Standard deviation.

*, $P < 0.05$; **, $P < 0.01$

†Values correspond from *Left* to *Right* to 1) nonreconstruction and 2) reconstruction of the ischial spines of Pelvis 1 (see also *SI Appendix* , Text S3). Z- Scores calculated using the values of the reconstruction of the spines.

‡Pubic length / Ischial Lenght x 100.

§Definition of variables from refs. 11, 26, 40-44.

¶Modern data from one European (Portuguese) sample, except for the "sacral lenght, curved", the "angulation of the sacrum" and the inlet, midplane and outlet circumferences from an American pooled sample (see *SI Appendix* ,Table S8).

‖Measurements taken on the left side of Pelvis 1 (AT-1000).

††Considering the first five elements of the sacrum.

Table S3. Character state and corresponding age-at-death of the SH Pelvis 1 individual

Region	Feature	Description	Criteria	Biological age	Chronological age
Pubic symphysis	Surface texture	Grained and pitted irregular surface	refs. 45-52	Middle to advanced adult	Above 45 years old
	Transverse organization	Absent			
	Ventral rampart formation	Complete			
	Symphyseal rim	Mostly eroded			
	Lipping	Moderate at the dorsal edge			
	Ventral margin	Irregular			
Auricular surface	Surface texture	Loss of coarse granulation to densification	refs. 53-55		
	Billowing/Striations	Some hardly distinct relicts (right os coxae)			
	Porosity	Limited micro- and macroporosity			
	Anterior margin	Irregular, onset of dull rim formation			
Acetabulum	Acetabular groove	Pronounced	ref. 56		
	Acetabular rim - shape	High dense crest (superior and posterior rim)			
	Acetabular rim - porosity	Rough appearance with macroporosity, but not destructured rim			
	Apex activity	Osteophyte (> 3 mm) covering the entire lunate horn			
	Acetabular fossa - activity	Deep fossa, extensive activity with loss of consistency within the fossa and partially destructed acetabular outer edges			
	Acetabular fossa - porosity	Base of micro- and macroporosities and some macroporosities with desctruction			

Table S4. Summary of the most relevant lumbo-pelvic traits in fossil and modern humans

		Lower Pleistocene *Homo*	European Middle Pleistocene *Homo*	Asian Middle Pleistocene *Homo*	African Middple Pleistocene *Homo*	Neandertals	Modern *Homo sapiens*
		KNM-ER 3228, OH 28, KNM-WT 15000, BSN49/P27, SK-853	Arago 44, Sima de los Huesos sample, Villafamés 2	Jinniushan	E. 719	La Chapelle-aux-Saints, La Ferrassie 1, Neandertal 1, Amud 1, Kebara 2, Shanidar 1, Shanidar 3, Shanidar 4, Tabun C1, Krapina sample	
Iliac crest shape in lateral anatomical view		Asymmetric relative to the highest point	Asymmetric relative to the highest point	Asymmetric relative to the highest point	?	Asymmetric relative to the highest point	Tendecy to symmetry relative to the highest point
ASIS projection in lateral view		Well beyond the AIIS	Well beyond the AIIS	Well beyond the AIIS	?	Well beyond the AIIS	Variable, typically behind the AIIS
AIIS having parallel walls		No	Yes	Yes	?	Yes	Variable, typically nonparallel walls
Supraacetabular sulcus		Well-depressed	Well-depressed	Well-depressed	Well-depressed	Well-depressed	Shallow to nondepressed
Number of iliac pillars		Variable	Two (ventral and lateral)	Two (ventral and lateral)?	At least one	Two (ventral and lateral)	Variable
Iliac Lateral Flaring		Large	Large	Large	Large?	Large	Small
Cotylosciatic region morphology (Posterior wall of the acetabulum)		Flat surface	Variable*	?	Flat surface	Flat surface	Blunted surface
Superior pubic ramus morphology at the obturator nerve sulcus		Thin and plate-like?†	Thin and plate-like	Thin and plate-like	?	Extremely thin and plate-like	Stout and bar-like
Degree of lordosis of the lumbar spine		?	Hypolordotic due to hyperkyphotic vertebral bodies	?	?	Hypolordotic due to hyperkyphotic vertebral bodies	Normal
Lumbar Transverse process	Length	Long?	Long	?	?	Long	Short
	Horizontal orientation (L2-L3)	Dorsolateral	Dorsolateral	?	?	Lateral	Dorsolateral
	Coronal orientation (L2-L3)	Lateral	Lateral	?	?	Cranial	Lateral
DV size of the vertebral canal in L4 and L5		Normal	Normal	?	?	Large	Normal

(ASIS) Anterior superior iliac spine; (AIIS) Anterior inferior iliac spine; (DV) Dorsoventral.
*SH sample: flat surface; Arago 44: blunted surface.
†From ref. 33, Fig. 3.

Table S5. Comparative values of the depth of the superior pubic ramus

Specimen		Value (mm)	Modern Male Z-score	Modern Female Z- score	Neandertal Z-score
SH sample					
SH Pelvis 1 (AT-1000)†		10.7	-1.9	-1.5	2.5*
Coxal I = AT-500+501+AT-708†§		9.0	-2.6**	-2.3*	0.8
AT-1006		10.3	-2.1*	-1.7	2.1*
AT-1535§		13.8	-0.6	0.0	5.6**
AT-1693+AT-1709†§		11.6	-1.5	-1.0	3.4**
AT-1701§		13.7	-0.7	0.0	5.5**
AT-1706†§		8.6	-2.8**	-2.5*	0.4
AT-1928+AT-1939†		10.3	-2.1*	-1.7	2.1*
AT-2502+AT-2508§		8.8	-2.7**	-2.4*	0.6
AT-3069		10.5	-2.0*	-1.6	2.3*
AT-3497+AT-3813+AT-3814		10.4	-2.0*	-1.6	2.2*
AT-3812+AT-3815+3816+AT-3820+AT-6233		9.7	-2.3*	-2.0	1.5
Mean ± SD *(range)(n)*		10.6 ± 1.6 (8.6/13.8)(12)			
Neandertals					
Amud 1		10.0			
Kebara 2		8.3			
Shanidar 1		7.0‡			
Tabun C1		6.8‡			
Krapina 208 (Cx.2)		8.9			
Krapina 209+212 (Cx.3+Cx.6)		8.2			
Krapina 255.10		8.2			
Mean ± SD *(range)(n)*		8.2 ± 1.0 (6.8/10.0)(7)			
Modern humans [European (Portuguese)]					
Males	*Mean ± SD* *(range)(n)*	15.3 ± 2.4 (9.3/22.9)(212)			
Females	*Mean ± SD* *(range)(n)*	13.8 ± 2.1 (8.8/18.4)(184)			

Depth of the superior pubic ramus according to ref. 41.
See *SI Appendix,* Tables S1, S8 for material information.
See *SI Appendix,* Table S2 footnote for modern Z-score calculation.
Neandertal Z-score = (SH value - Neandertal mean) / Neandertal SD.
(SD) Standard deviation.
*, $P < 0.05$; **, $P < 0.01$
†Superior pubic ramus section previously figured in ref. 13, Fig. 3.
‡Mean value between the left and right ossa coxae.
§Immature individuals (see *SI Appendix* , Table S8 for details).

Table S6. Comparative osteometry of the SH Pelvis 1 individual's lumbar vertebrae

Vertebra	Region	Variable	Martin's vertebral number†	**SH Pelvis 1 individual‡**	Z-score 1 (vs European)	Z-score 2 (vs Euroamerican)	SH VL12(L5)	European (Recent Spaniards) males	European American (Hamann-Todd) males	Kebara 2	Shanidar 3	La Chapelle-aux-Saints
								Mean ± SD (range)(n)	*Mean ± SD (range)(n)*			
L2	Vertebral body	Ventral cranio-caudal diameter	M1	(21.6)	-2.85**	-4.12**	-	26.12 ± 1.58 (23.2/29.5)(29)	27.78 ± 1.50 (25.0/30.7)(27)	23.8	24.8	-
		Dorsal cranio-caudal diameter	M2	(27.5)	0.15	-0.29	-	27.78 ± 1.47 (24.5/30.1)(30)	27.96 ± 1.61 (25.0/31.1)(28)	27.9	(29.5)	-
		Cranial dorsoventral diameter	M4	(37.0)	2.84**	2.24*	-	31.56 ± 1.91 (29.2/35.8)(28)	31.82 ± 2.31 (26.5/36.5)(27)	34.6	(34.3)	-
	Vertebral canal	Dorsoventral diameter	M10	(16.5)	0.07	-0.04	-	16.43 ± 1.13 (13.0/18.6) (31)	16.55 ± 1.26 (14.2/18.6)(28)	16.9	-	-
L3	Whole vertebra	Maximum DV diameter		90.4	2.87**	1.53	-	81.04 ± 3.27 (74.4/87.0)(26)	83.73 ± 4.37 (74.8/91.4)(25)	-	82.5	-
	Vertebral body	Ventral cranio-caudal diameter	M1	21.4	-3.43**	-6.10**	-	26.88 ± 1.60 (24.0/30.2)(28)	28.76 ± 1.21 (26.3/31.1)(28)	23.4	27.0	-
		Dorsal cranio-caudal diameter	M2	(27.5)	0.45	-0.13	-	26.82 ± 1.51 (24.6/30.0)(30)	27.75 ± 1.96 (24.1/31.7)(28)	28.0	29.2	27.2
		Cranial dorsoventral diameter	M4	(38.5)	3.65**	2.55*	-	32.39 ± 1.67 (29.4/36.4)(28)	32.68 ± 2.28 (28.7/38.1)(28)	36.4	33.1	-
		Medial transverse diameter	M9	48.6	3.33**	2.17*	-	40.22 ± 2.52 (36.7/44.6)(28)	41.69 ± 3.19 (36.9/50.6)(28)	40.1	-	45.0
	Transverse process	Length (R/L)		46.3/-	3.35**/-	2.85**/-	-	35.16 ± 3.32 (28.7/41.1)(24)	35.35 ± 3.88 (29.4/43.2)(21)	37.3/39.7	-	-
		Horizontal angle (R/L)		111.2/-	-0.50	-	-	113.7 ± 4.96 (104.5/123.6)(25)	-	93.4/86.8	-	-
L4	Whole vertebra	Maximum DV diameter		83.1	0.95	0.16	-	79.75 ± 3.54 (72.8/87.3)(28)	82.35 ± 4.56 (72.7/90.4)(28)	-	-	-
	Vertebral body	Ventral cranio-caudal diameter	M1	21.5	-3.60**	-5.22**	-	27.22 ± 1.59 (22.4/29.8)(24)	28.69 ± 1.38 (26.1/31.9)(27)	26.0	28.9	-
		Dorsal cranio-caudal diameter	M2	(26.2)	0.16	-0.23	-	26.22 ± 1.66 (23.8/29.8)(29)	26.74 ± 2.38 (22.0/31.4)(28)	27.9	29.0	26.1
		Cranial dorsoventral diameter	M4	36.2	1.44	0.74	-	32.61 ± 2.50 (29.3/38.4)(24)	33.65 ± 3.44 (29.9/48.1)(28)	35.4	33.8	-
		Medial transverse diameter	M9	49.0	2.75**	1.55	-	42.93 ± 2.21 (39.8/47.5)(30)	43.91 ± 3.27 (38.0/53.2)(28)	43.1	45.3	49.5
	Vertebral canal	Dorsoventral diameter	M10	14.6	-0.60	-0.86	-	15.49 ± 1.50 (13.1/20.3)(31)	16.23 ± 1.90 (13.7/20.7)(28)	19.0	21.3	-
L5	Whole vertebra	Maximum DV diameter		86.2	3.26**	2.23*	(87.5)	75.45 ± 3.30 (69.5/83.4)(28)	76.80 ± 4.22 (69.8/82.7)(25)	(81.0)	-	-
	Vertebral body	Ventral cranio-caudal diameter	M1	(27.1)	-0.28	-1.46	28.1	27.59 ± 1.72 (23.3/30.4)(28)	29.08 ± 1.36 (26.4/32.2)(28)	29.8	30.6	(29.0)
		Dorsal cranio-caudal diameter	M2	25.8	1.17	0.1	(24.0)	24.05 ± 1.50 (21.8/27.5)(28)	24.58 ± 2.00 (20.8/28.7)(28)	24.5	25.3	24.6
		Cranial dorsoventral diameter	M4	(35.0)	0.77	0.42	36.0	33.34 ± 2.16 (28.9/37.9)(28)	34.03 ± 2.31 (30.3/39.8)(28)	34.9	36.1	(38.0)
		Medial transverse diameter	M9	52.5	2.16*	1.04	46.5	47.24 ± 2.44 (42.0/51.2)(29)	48.69 ± 3.66 (41.7/57.4)(28)	43.9	47.5	47.0
	Vertebral canal	Dorsoventral diameter	M10	17.2	0.21	0.02	17.9	16.80 ± 1.89 (11.4/21.0)(31)	17.16 ± 2.51 (13.1/22.5)(26)	23.0	22.4	-
	Transverse process	Length (R/L)		-/(40.5)	-/(2.60)**	-/(2.79)**	-/44.5	32.24 ± 2.27 (29.0/37.1)(22)	32.91 ± 2.73 (27.7/37.7)(26)	39.1/40.3	36.7/38.2	-

Measurements given in milimeters and sexagesimal degrees. Estimations in parentheses.
See *SI Appendix,* Table S8 for material information.
See *SI Appendix,* Table S2 footnote for modern Z-score calculation.
(DV) Dorsoventral; (R) Right; (L) Left; (SD) Standard deviation.
*, $P < 0.05$; **, $P < 0.01$
†According to ref. 32.
‡The first lumbar vertebra of the SH Pelvis 1 individual is not complete enough to measure it.

Table S7. Sagittal spino-pelvic morphometry in modern humans

Sample	Sex	SAO	PI	Vertebral wedging*				
				L1	L2	L3	L4	L5
European American (Hamman-Todd) *Mean ± SD (range)(n)*	♂	49.45 ± 9.52 (28.0/77.0)(147)	52.15 ± 12.33 (18.3/83.7)(147)	1.03 ± 1.18 (-1.7/3.0)(27)	0.15 ± 1.22 (-2.1/2.8)(27)	-0.89 ± 1.25 (-3.0/1.8)(28)	-1.76 ± 1.64 (-5.3/1.2)(27)	-3.80 ± 1.57 (-7.0/-0.9)(28)
European American (Hamman-Todd) *Mean ± SD (range)(n)*	♀			0.66 ± 1.38 (-3.2/3.9)(25)	-0.28 ± 1.45 (-2.5/3.4)(27)	-1.21 ± 1.13 (-3.5/1.6)(27)	-2.72 ± 1.31 (-5.4/0.0)(27)	-5.06 ± 1.74 (-8.6/-2.0)(28)
African American (Hamman-Todd) *Mean ± SD (range)(n)*	♂	48.16 ± 10.02 (18.0/73.0)(116)	55.98 ± 12.19 (27.6/88.5)(116)					
European (Recent Spaniards) *Mean ± SD (range)(n)*	♂			2.31 ± 1.04 (0.3/4.5)(24)	1.03 ± 0.94 (-0.6/2.6)(28)	-0.08 ± 1.27 (-2.4/2.3)(28)	-0.80 ± 1.19 (-2.5/2.0)(24)	-3.14 ± 1.35 (-5.6/-0.5)(26)

See *SI Appendix,* Text S6, Table S8, Fig. S6 for material and methods information.

(SAO) Sacral anatomical orientation; (PI) Pelvic incidence; (SD) Standard deviation.

*Positive and negative values indicate ventral (kyphotic vertebral bodies) and dorsal (lordotic vertebral bodies) wedging, respectively.

Table S8. Comparative sample

Specimen/Collection	Region*	Material (Repository)
Lower Pleistocene *Homo*		
BSN49/P27	Pelvis	ref. 33
KNM-ER 3228	Pelvis	Cast (Centro UCM-ISCIII de evolución y comportamiento humanos, Madrid, Spain)
KNM-WT 15000	Pelvis and lumbar vertebrae	Cast (Centro UCM-ISCIII de evolución y comportamiento humanos, Madrid, Spain)
OH 28	Pelvis	Cast (Centro UCM-ISCIII de evolución y comportamiento humanos, Madrid, Spain)
SK-853	Lumbar vertebra	ref. 2
Middle Pleistocene *Homo*		
Arago 44	Pelvis	Cast (Centro UCM-ISCIII de evolución y comportamiento humanos, Madrid, Spain)
Broken Hill E. 719	Pelvis	Cast (Department of Anatomy and Anthropology, Tel Aviv University, Tel Aviv, Israel)
Jinniushan 1	Pelvis	refs. 24, 25, 57, 58
Villafamés 2 (CTF 2)	Pelvis	Original (Servicio de Investigaciones Arqueológicas y Prehistóricas de la Diputación de Castellón, Castellón, Spain)
Sima de los Huesos sample †		Originals (Junta de Castilla y León, Spain)
Pelvis 2 = (Coxal II=AT-800[a,b,c])+AT-1234+AT-2721	Quite complete left os coxae and first sacral vertebra	+ Surface scan‡
Coxal I[a,b,c] = AT-500[a,b,c]+AT-501[a]+AT-708[a]	Quite complete right os coxae	
Coxal III = AT-3807+AT-3808+AT-3809+AT-3300	Quite complete left os coxae	
Coxal V = AT-1004[b,c]+(AT-1819+AT-6235)	Quite complete right os coxae	
[VL4(L4) = AT-3730+AT-3731][d]	Vertebral body and fragmentary neural arch of a fourth lumbar vertebra (L4)	
[VL10(L1) = AT-875+AT-131+AT-3010+AT-3012][d]	Nearly complete first lumbar vertebra (L1)	
[VL12(L5) = AT-3337+AT-3728+AT-3732+AT-3740+AT-3848+AT-5687][d]	Nearly complete fifth lumbar vertebra (L5)	
[VL13(L5) = AT-1129+AT-1225+AT-3980][d]	Fragmentary L5	
[VL18(L2) = AT-4188+AT-5578+AT-5673][d]	Nearly complete second lumbar vertebra (L2)	
Femur X[b,c] = AT-612+AT-1800+AT-4724	Complete left femur	
Femur XII = AT-665+AT-855	Complete right femur	
Femur XIII[b] = AT-999[b]+AT-2944+AT-2945	Complete left femur	
AT-322[a,b]	Sacrum with its first two partially preserved vertebrae	
AT-659[a]+AT-3817	Right iliac fragment, preserving part of the pillar and the portion of the crest behind the tubercle	
AT-1005	Nearly complete sacrum	
AT-1006[c]	Right pubic body and superior pubic ramus	
AT-1570	Complete first coccygeal vertebra	
AT-1535	Left proximal portion of the superior pubic ramus	
AT-1693[c]+AT-1709	Nearly complete left pubic bone	
AT-1701	Right proximal portion of the superior pubic ramus	
AT-1706[c]	Right proximal portion of the superior pubic ramus	
AT-1830	Body of a middle (second to fourth) coccygeal vertebra	
AT-1928[c]+AT-1939	Right proximal portion of the superior pubic ramus	
AT-2500[c]+AT-4292+AT-6236	Quite complete left pubis	
AT-2502+AT-2508	Nearly complete right pubic bone	
AT-3069	Fragment of the left proximal portion of the superior pubic ramus	
AT-3497+AT-3813+AT-3814	Nearly complete left pubic bone	
AT-3711+AT-4200+AT-4350	Quite complete sacrum	
AT-3812+AT-3815+3816+AT-3820+AT-6233	Fragmentary right os coxae	
AT-3853	Complete apical (third to fifth) coccygeal vertebra	
AT-4306	Body of a middle (second to fourth) coccygeal vertebra	
AT-4208	Complete first coccygeal vertebra	
AT-6239	Quite complete first coccygeal vertebra	
AT-6240	Complete middle (second to fourth) coccygeal vertebra	

Table S8. Comparative sample (continued)

Specimen/Collection	♂ (*n*)	♀ (*n*)	Region*	Material (Repository)
Homo neanderthalensis				
Amud 1			Pelvis	Original (Department of Anatomy and Anthropology, Tel Aviv University, Tel Aviv, Israel)
Kebara 2			Pelvis and lumbar vertebrae	Original (Department of Anatomy and Anthropology, Tel Aviv University, Tel Aviv, Israel), cast (Centro UCM-ISCIII de evolución y comportamiento humanos, Madrid, Spain), and ref. 6
Krapina sample				Originals (Croatian Museum of Natural History, Zagreb, Croatia)
Krapina 207 (Cx.1)			Pelvis	
Krapina 208 (Cx.2)			Pelvis	
Krapina 209+212 (Cx.3+Cx.6)			Pelvis	
Krapina 255.1			Pelvis	
Krapina 255.6			Pelvis	
Krapina 255.7			Pelvis	
Krapina 255.8			Pelvis	
Krapina 255.9			Pelvis	
Krapina 255.10			Pelvis	
La Chapelle-aux-Saints			Pelvis and lumbar vertebrae	Original (Musée de l'Homme, Paris, France)
La Ferrassie 1			Pelvis	ref. 59
Neandertal 1			Pelvis	Cast (Department of Anatomy and Anthropology, Tel Aviv University, Tel Aviv, Israel)
Shanidar 1			Pelvis	ref. 9
Shanidar 3			Pelvis and lumbar vertebrae	Original (Department of Anthropology, Natural History Museum, Smithsonian Institution, Washington DC, USA) and ref. 9
Shanidar 4			Pelvis	ref. 9
Subalyuk			Pelvis	Cast (Department of Anatomy and Anthropology, Tel Aviv University, Tel Aviv, Israel)
Tabun C1			Pelvis	CT-scan (from ref. 23) and refs. 23, 41
Modern *Homo sapiens*	♂ (*n*)	♀ (*n*)		
African American (Hamman-Todd)	116	-	Pelvis	ref. 28
American pooled sample §	345	-	Pelvis	ref. 26
European (Portuguese)	221	187	Pelvis	Dry bone (Instituto de Antropologia de la Universidade de Coimbra, Coimbra, Portugal) and ref. 40
European (Recent Spaniards)	213	-	Pelvis and lumbar vertebrae	Dry bone (Laboratorio de Evolución Humana, Universidad de Burgos, Burgos, Spain)
European (Medieval Spaniards)	58	-	Pelvis	Dry bone (Laboratorio de Evolución Humana, Universidad de Burgos, Burgos, Spain)
European American (Hamman-Todd)	173	35	Pelvis and lumbar verterbrae	Dry bone (Cleveland Museum of Natural History, Hamann-Todd Collection, Cleveland, USA) and ref. 28
European American (Iowa)	6	-	Lumbar vertebrae	Dry bone (Department of Anthropology, University of Iowa, Iowa City, USA)

*The pelvic region includes sacrum and os coxae.

†All specimens showing completely mature state (based on the epiphyseal closure, bone appearance, relative size, and modifications of the symphyseal and auricular surfaces), with the exception of: Coxal I (triradiate cartilage stage - fusing), Coxal V (triradiate cartilage stage - completely ossified; iliac crest epiphysis - unfused; ischial tuberosity epiphysis - ossifing), AT-1535 (anterior acetabular epiphysis - not ossified; size - large), AT-1693+AT-1709 (anterior acetabular epiphysis - completely ossified; pubic symphysis - well-marked ridge-and-furrow appearance), AT-1701 (anterior acetabular epiphysis - ossifing; size - large), AT-1706 (anterior acetabular epiphysis - almost complete ossification) and AT-2502+AT-2508 (pubic symphysis - well-marked ridge-and-furrow appearance; size - large)

(a) Previously referenced in ref. 60.
(b) Previously published in refs. 37, 38.
(c) Previously published in ref. 13.
(d) Previously referenced in ref. 39.

‡ See *SI Appendix* , Text S7

§Combined data from four Amerindians (Indian, Pecos Pueblo, Liben, Haida), one European American and one African American male populations (see ref. 44 for further details).

Supporting Information IV: References

1. Pilbeam D (2004) The anthropoid postcranial axial skeleton: comments on development, variation, and evolution. *J Exp Zoolog B Mol Dev Evol* 302B:241-267.
2. Robinson JT (1972) *Early Hominid Posture and Locomotion* (University of Chicago Press, Chicago).
3. Latimer B, Ward C (1993) *The Nariokotome* Homo erectus *Skeleton*, eds. Walker A, Leakey R (University Press, Cambridge, MA), pp. 266-293.
4. McCollum M, Rosenman BA, Suwa G, Meindl RS, Lovejoy CO (2010) The vertebral formula of the last common ancestor of african apes and humans. J Exp Zoolog B Mol Dev Evol 314B:123-124.
5. Haeusler M, Martelli SA, Boeni T (2002) Vertebral numbers of the early hominid lumbar spine. *J Hum Evol* 43:621-643.
6. Arensburg B (1991) *The Mousterian Skeleton of Kebara 2* (Translated from French), eds Bar-Yosef O, Vandermeersch B (Éditions du CNRS, Paris), pp 113-147.
7. Ogilvie MD, Hilton CE, Ogilvie CD (1998) Lumbar anomalies in the Shanidar 3 Neandertal. *J Hum Evol* 35:597-610.
8. Heim JL (1976) *The Human Fossils from La Ferrassie. I. The Site. The Adult Skeletons (Cranium and Trunk)* (Translated from French) (Masson, Paris).
9. Trinkaus E (1983) *The Shanidar Neanderthals* (Academic Press, New York).
10. Been E, Peleg S, Marom A, Barash, A (2010) Morphology and function of the lumbar spine of the Kebara 2 Neandertal. *Am J Phys Anthropol* 142:549-557.
11. Genovés S (1959) Sexual differences in the os coxae (Translated from Spanish). PhD. Thesis (Universidad Autónoma de México).
12. Sgambati E, Stecco A, Capaccioli L, Brizzi E (1996) Morphometric evaluation of the symphysis pubis joint. *Ital J Anat Embryol* 101**:**195-201.
13. Arsuaga JL*, et al.* (1999) A complete human pelvis from the Middle Pleistocene of Spain. *Nature* 399**:**255-258.
14. Carretero JM*, et al.* (2004) *Tribute to Emiliano Aguirre. Paleoanthropology* (Translated from Spanish), eds Baquedano E, Rubio S (Museo Arqueológico Regional de la Comunidad de Madrid, Alcalá de Henares), pp 120-135.
15. McHenry H (1975) Biomechanical interpretation of the early hominid hip. *J Hum Evol* 4:343-355.
16. Feldesman MR, Kleckner JG, Lundy JK (1990) The femur/stature ratio and estimates of stature in mid- and late-Pleistocene fossil hominoids. *Am J Phys Anthropol* 83**:**359-372.
17. Trotter M, Glesser GC (1952) Estimation of stature from long bones of American Whites and Negroes. *Am J Phys Anthropol* 10**:**463-514.
18. Trotter M, Glesser GC (1958) A re-evaluation of estimation of stature based on measurements of stature taken during life and of long bones after death. *Am J Phys Anthropol* 16**:**79-123.
19. Ruff CB, Trinkaus E, Holliday TW (1997) Body mass and encephalization in Pleistocene *Homo*. *Nature* 387**:**173-176.
20. Ruff CB, Niskanen M, Junno J-A, Jamison P (2005) Body mass prediction from stature and bi-iliac breadth in two high latitude populations, with implication to earlier higher latitude humans. *J Hum Evol* 48**:**321-434.
21. Arsuaga JL, Martínez I, Gracia A (2001) Phylogenetic analysis of the hominids

from the Sierra de Atapuerca (Sima de los Huesos and Gran Dolina TD-6): The cranial evidence (Translated from French). *Anthropologie* 105**:**161-178.
22. Martin Rd (1981) Relative brain size and basal metabolic rate in terrestrial vertebrates. *Nature* 293**:**56-60.
23. Weaver TD, Hublin JJ (2009) Neadertal birth canal shape and the evolution of human childbirth. *Proc Natl Acad Sci USA* 106**:**8151-8156.
24. Rosenberg KR (2007) Neandertal pelvic remains from Krapina: Peculiar or primitive? *Period Biol* 109**:**387-392.
25. Rosenberg K, Zuné L, Ruff CB (2006) Body size, body proportions, and encephalization in a Middle Pleistocene archaic human from northern China. *Proc Natl Acad Sci USA* 103**:**3552-3556.
26. Tague RG (1992) Sexual dimorphism in the human bony pelvis, with a consideration of the neandertal pelvis from Kebara Cave, Israel. *Am J Phys Anthropol* 88**:**1-21.
27. Ponce De León MS*, et al.* (2008) Neanderthal brain size at birth provides insights into the evolution of human life history. *Proc Natl Acad Sci USA* 105**:**13764-13768.
28. Peleg S*, et al.* (2007) Orientation of the human sacrum: Anthropological perspectives and methodological approaches. *Am J Phys Anthropol* 133**:**967-977.
29. Legaye J (2007) The femoro-sacral posterior angle: An anatomical sagittal pelvic parameter usable with dome shaped sacrum. *Eur Spine J* 16**:**219-225.
30. Duval-Beaupère G, Schmidt C, Cosson P (1992) A barycentremetric study of the sagittal shape of spine and pelvis: The conditions requiered for an economic standing position. *Ann Biomed Eng* 20**:**451-462.
31. Digiovanni BF, Scoles PV, Latimer B (1989) Anterior extension of the thoracic vertebral bodies in Scheuermann's kyphosis. An anatomic study. *Spine (Phila Pa 1976)* 14**:**712-716.
32. Braüer, G (1988) *Anthropology. Handbook of Comparative Human Biology* (Translated from German), ed Knussmann R, (Gustav Fischer, Stuttgart), pp. 160-232.
33. Simpson SW*, et al.* (2008) A female *Homo erectus* pelvis from Gona, Ethiopia. *Science* 322**:**1089-1091.
34. Takemitsu Y*, et al.* (1988) Lumbar degenerative kyphosis. Clinical, radiological and epidemiological studies. *Spine (Phila Pa 1976)* 13:1317-1326.
35. Barrey C, Jund J, Noseda O, Roussouly P (2007) Sagittal balance of the pelvis-spine complex and lumbar degenerative disease. A comparative study about 85 cases. *Eur Spine J* 16:1459-1467.
36. Jang JS, Lee SH, Min JH, Han KM (2007) Lumbar degenerative kyphosis: Radiologic analysis and classifications. *Spine (Phila Pa 1976)* 32:2694-2699.
37. Arsuaga JL*, et al.* (1997) Size Variation in Middle Pleistocene Humans. *Science* 277**:**1086-1088.
38. Lorenzo C*, et al.* (1998) Intrapopulational body size variation and cranial capacity variation in Middle Pleistocene humans: The Sima de los Huesos sample (Sierra de Atapuerca, Spain). *Am J Phys Anthropol* 106**:**19-33.
39. Gómez-Olivencia A (2009) Paleobiological research on the vertebral column and the thoracic cage of Pleistocene fossil humans, with special reference to the fossils from the Sierra de Atapuerca (Translated from Spanish). PhD. Thesis (University of Burgos).
40. Serra JA (1938) The Portuguese pelves. Morphology of the human pelvis (Translated from Portuguese). *Contrib Estudo Anthropol Port* 3**:**1-13.
41. McCown T, Keith A (1939) *The Stone Age of Mount Carmel. The Fossil Human*

Remains from the Levallois-Mousterian (Clarendon Press, Oxford).
42. Sauter MR, Privat F (1954-55) Regarding a new metrical approach to the sexual assessment of the bony pelvis (Translated from French). *Bull. Soc. Suisse Anthrop. Ethnol.* 31**:**60-84.
43. Arsuaga JL (1985) Anthropology of the os coxae: Evolution, sexual dimorphism and variability (Translated from Spanish). PhD. Thesis (Complutense University).
44. Tague RG (1989) Variation in pelvic size between males and females. *Am J Phys Anthropol* 80**:**59-71.
45. Todd TW (1920) Age changes in the pubic bone: I. The white male pubis. *Am J Phys Anthropol* 3**:**347-470.
46. Todd TW (1921a) Age changes in the pubic bone: II. The pubis of the male Negro-White hybrid. *Am J Phys Anthropol* 4**:**1-25.
47. Todd TW (1921b) Age changes in the pubic bone: III. The pubis of the White female. *Am J Phys Anthropol* 4**:**26-39.
48. Todd TW (1921c) Age changes in the pubic bone: IV. The pubis of the female Negro-White hybrid. *Am J Phys Anthropol* 4**:**40-57.
49. Mckern TW, Stewart TD (1957) *Skeletal Age Changes in Young American males, Analysed from the Standpoint of Age Identification* (U.S. Army, Quartermasters Research and Development Command, Natick, MA).
50. Gilbert BM, Mckern TW (1973) A method for aging the female os pubis. *Am J Phys Anthropol* 38**:**31-38.
51. Meindl RS, Lovejoy CO, Mensforth RP, Walker RA (1985) A revised method of age determination using the os pubis, with a review and tests of accuracy of other current methods of pubis symphyseal aging. *Am J Phys Anthropol* 68**:**29-45.
52. Brooks S, Suchey JM (1990) Skeletal age determination based on the os pubis: A comparision of the Acsádi-Nemeskéri and Suchey-Brooks methods. *Hum evol* 5**:**227-238.
53. Lovejoy CO, Meindl RS, Targue RG, Latimer BM (1985) Chronological metamorphosis of the auricular surface of the ilium: A new method for the determination of adult skeletal age at death. *Am J Phys Anthropol* 68**:**15-28.
54. Buckberry JL, Chamberlain AT (2002) Age estimation from the auricular surface of the ilium: A revised method. *Am J Phys Anthropol* 119**:**231-239.
55. Igarashi Y, Uesu K, Wakebe T, Kanazawa E (2005) New method for estimation of adult skeletal age at death from the morphology of the auricular surface of the ilium. *Am J Phys Anthropol* 128**:**324-339.
56. Rissech C, Estabrook GF, Cunha E, Malgosa A (2006) Using the acetabulum to estimate age at death of adult males. *J Foren Sci* 51**:**213-229.
57. Rosenberg K (1998) *Neandertals and Modern Human in Western Asia*, eds. Akazawa T, Aoki K, Bar-Yosef O (Plenum, New York), pp. 367-379.
58. Lu Z (2003) *Current Research in Chinese Pleistocene Archaeology*, eds. Shen C, Keates SG (Archaeopress, Oxford), pp. 127-136.
59. Heim JL (1982) *The Human Fossils from La Ferrassie. II. The Adult Skeletons: Appendicular Skeleton* (Translated from French) (Masson, Paris).
60. Carretero JM (1994) Research on the two girdles and the upper limb of the skeleton of the hominids from Sima de los Huesos, Sierra de Atapuerca, Burgos (Translated from Spanish). PhD. Thesis (Complutense University).